Peperites: Insight into the Submarine Eruptions within Walash Volcanosedimentary Group, Mawat Area, Iraqi Kurdistan Region

Jabbar M. A. Qaradaghi and Tola A. Mirza

Department of Geology, College of Science, Sulaimani University,
Sulaimani, Kurdistan Region–F.R, Iraq

Abstract—**Peperites are volcanosedimentary materials generated by the mingling of magma and unconsolidated wet sediments. They have unique insights into submarine volcanisms and the tectonic environments where they form. For the 1st time, the authors identified two types of peperites (blocky and fluidal) hosted by micritic limestone rocks in the Walash Volcanosedimentary Group of the Mawat area, Kurdistan Region-Iraq. They are designated as peperitic facies one and two (PF1 and PF2) and consist of black basaltic rocks mixed with chocolate-brown micritic limestone rocks. Their abundance demonstrates the contemporaneity of deep marine sediment deposition and submarine volcanism during Walash's nascent arc. Despite hydrothermal alteration, the basaltic rocks retained their magmatic textures. Basaltic rocks comprise mainly albite, anorthite, diopside, hematite, and alkali-feldspar. Calcite dominates micritic limestone rocks, while quartz is minor. Based on geochemical data, igneous sections are basaltic rocks with tholeiitic series that are strongly enriched in Light Rare Earth Elements with low concentration ratios of (La/Yb) and (Sr/Y), indicating geochemical affinity to normal island arc basalt with a primitive arc signature. Furthermore, their formation is thought to be caused by partial melting of subducted slabs deep within 30 km and the associated derived fluids above the subducted slab. Thirteen species of planktonic foraminifera (Morozovella) are identified through paleontological research and biostratigraphy. Using these various tools lead the authors to illustrate the tectonic setting of the formation of peperitic rocks in arc fronts of the subducted Walash arc during the Middle to Late Paleocene (60 Ma).**

Index Terms—Mawat, Paleocene, Peperite, Primitive Arc, Volcanic Arc, Walash.

I. Introduction

The term "peperite," comes after "peperino," first used by (Scrope, 1827) to describe clastic rocks from the Limagne d' Auvergne region of central France (now considered the type locality for "peperite"). It comprises mixtures of wet sediment or lacustrine limestone and basalt (Skilling, et al., 2002). Peperite is a combined rock formed essentially *in situ* by the disintegration of magma which intrudes and mingles with unconsolidated or poorly consolidated, typically wet sediment (Busby-Spera and White, 1987; White, Mcphie and Skilling, 2000; Skilling, et al., 2002; Brown and Bell, 2007; El Desoky and Shahin, 2020). However, most peperites described as basaltic extrusion involve relatively fine-grained sediment (White and Busby-Spera, 1987; Hanson, 1991; Boulter, 1993; Hanson and Wilson, 1993; Rawlings, 1993; Brooks, 1995; Goto and McPhie, 1996; Hanson and Hargrove, 1999; Skilling, et al., 2002; Waichel, et al., 2007; Branney, et al., 2008; Palinkaš, et al., 2008; Chen, et al., 2013; Famelli, et al., 2021; Bann, Jones and Graham, 2022). While few exceptions involve basaltic extrusions into coarse-grained host sediment (Wilson, 1991; Squire and McPhie, 2002). Peperite may extend its range from minor occurrences adjacent to igneous extrusions up to deposits with quantities of several km^3 (Brown and Bell, 2007). Texturally, peperites have different juvenile clast morphologies, including blocky and fluidal types, and numerous magma-sediment relationships (Busby-Spera and White, 1987). Peperite may occur in any tectonic environment, where magmatism and sedimentation are contemporaneous, frequently in arc-related and other volcanosedimentary sequences (Hanson and Hargrove, 1999; Mueller, Garde and Stendal, 2000; Skilling, et al., 2002; Dadd and Van Wagoner, 2002; Templeton and Hanson, 2003; Nemeth, Breitkreutz and Wilke, 2004; Chen, et al., 2016; Fontboté, 2019; Mawson, White and Palin, 2020). Consequently, petrologists have defined peperites in different ways, some authors may mistakenly define this rock as sedimentary rock, while others more properly define peperites as a combined volcano-sedimentary succession (White, McPhie and Skilling, 2000; Skilling, et al., 2002; Brown and Bell, 2007; Chen, et al., 2016; Krobicki, 2018; Krobicki, et al., 2019; Memtimin, et al., 2020).

The Walash Group was first named by Bolton (1958) and later subjected to numerous studies (e.g., Aziz, 1986; Jassim and Goff, 2006; Al-Banna and Al-Mutwali, 2008; Koyi, 2009; Ali, 2012; Al-Qayim, Ghafor and Jaff, 2012; Ali and Aswad, 2013; Ali, et al., 2013; Aswad, et al., 2013; Al-

ARO-The Scientific Journal of Koya University
Vol. XI, No. 2 (2023), Article ID: ARO.11363. 23 pages
DOI: 10.14500/aro.11363
Received: 27 August 2023; Accepted: 19 October 2023
Regular research paper: Published: 22 November 2023
Corresponding author's e-mail: jabbar.faraj@univsul.edu.iq

http://dx.doi.org/10.14500/aro.11363

Qayim, Ghafor and Jaff, 2014; Ali, et al., 2017; Koshnaw, et al., 2017; Karim and Hamza, 2021). Aziz (1986) studied the geochemistry and petrogenesis of the volcanic rocks within the Walash Volcanosedimentary Group (WVSg) for the first time, and he concluded that the volcanic rocks of the Walash composed of basalts and andesites, which display tholeiitic to calc-alkaline affinity, formed as a result of the subduction of the oceanic crust beneath the Iranian microcontinent. Previously, the ^{40}Ar-^{39}Ar geochronological data suggested an age of 43–32 Ma for the volcanic rocks of Walash in the Mawat ophiolite complex (Aswad, et al., 2013). Despite the aforementioned studies for WVSg, it is reasonable to do more meticulous petrological studies as it is the most complex volcanosedimentary unit in the Iraqi Zagros Suture Zone (IZSZ).

The occurrence of basaltic pillow lava, peperitic rocks, and host micritic carbonate rocks together within the lower part of WVSg is designated as the peperitic facies (PF) in this study. The primary goals of our research are to use peperite and basaltic rock compositions obtained from the WVSg in the Mawat area to reconstruct the tectonic setting of the basaltic rocks within the aforementioned volcanosedimentary group. In addition to covering the occurrence and genesis of peperites in the Mawat area within WVSg.

II. Tectonic Setting of the Region

The Zagros orogeny is an active orogeny that includes the Zagros mountains, which formed as the Arabian and Eurasian plates collided (Agard, et al., 2011; Austermann and Iaffaldano, 2013; Elias, Sissakian and Al-Ansari, 2018). Tectonically, the Zagros orogen is divided into four subparallel divisions, which are the Urumieh-Dokhtar Magmatic Arc; the Sanandaj-Sirjan Zone; the Zagros Fold-Thrust Belt and the Mesopotamian Foreland Basin (Alavi, 2004; Mohammad, et al., 2014; English, et al., 2015). Iraq also is a part of the Zagros orogeny. It is divided into different tectonic zones, which are Zagros Suture Zone (ZSZ), Unstable shelf, and Stable shelf. The studied area is located within the Penjween Walash sub-zone, which is a part of the IZSZ (Jassim and Goff, 2006) (Fig. 1). Jassim and Goff, (2006) defined the Penjween-Walash subzone as a unit of the main (Central) Neo-Tethys, which consists of volcanosedimentary sequences formed during Cretaceous Ocean spreading in the Neo-Tethys and Paleogene arc volcanics and syn-tectonic basic intrusions formed during the ocean's final closure. Thus, the oceanic sediments were deposited on both Arabian and Iranian microplates during the middle Paleocene. Later, Zagros orogeny was followed by the late Eocene 38 Ma continent-continent collision of the Arabian plate with

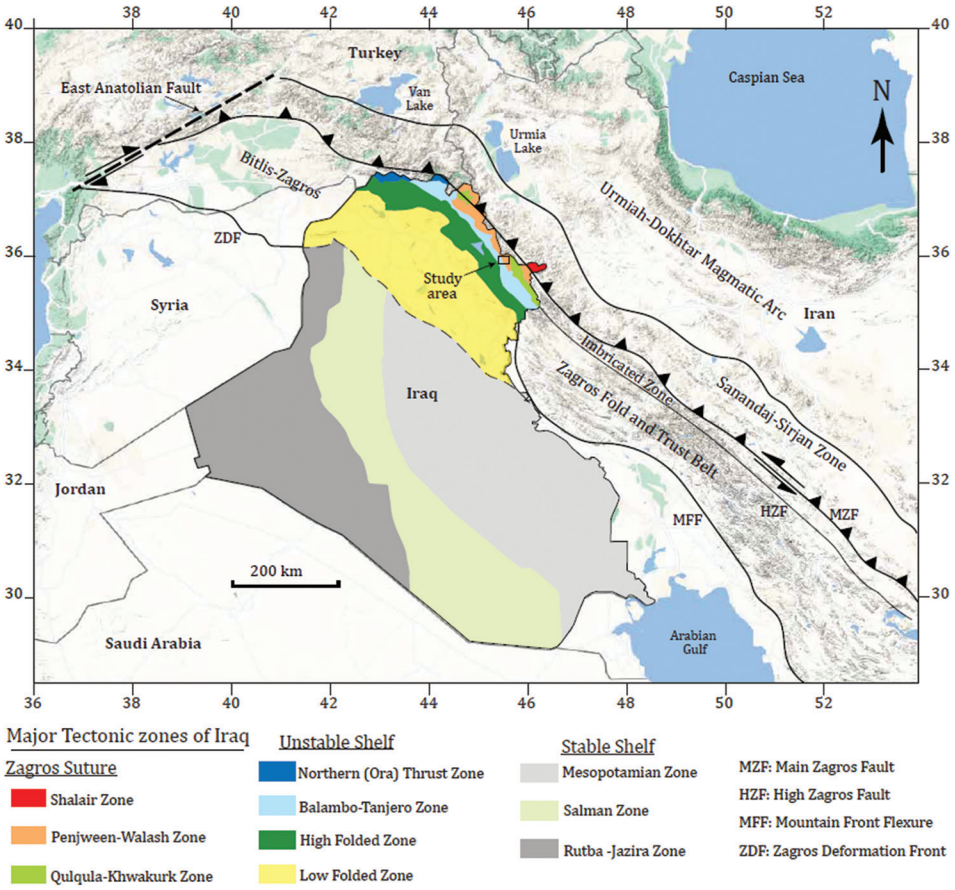

Fig. 1. Tectonic map of the studied area illustrating the tectonic division of Kurdistan and Iraq after (Jassim and Goff, 2006) and surroundings after (Alavi, 2004; English, et al., 2015).

Eurasia (Mohammad, et al., 2014). Furthermore, in the study area, the WVSg exposed in the Thrust Zone and the Mawat nappe stack consists of two allochthonous sheets, namely, the upper and lower allochthonous thrust sheets (Aswad et al., 2011; Aziz et al., 2011a). The lower allochthonous thrust sheet consists of Walash volcanosedimentary rocks, which undergo lateral transitions to the Naopurdan sedimentary group, thereby forming the Walash-Naopurdan allochthonous thrust sheet.

Peperite literature along the Zagros orogeny (Turkey-Iraq-Iran) is rare. Recently, Nouri et al., (2017) have recorded peperites within western Iran along the ZSZ. As well as Erkül, Helvaci and Sözbilir, (2006) recorded peperites within Miocene units in Western Turkey. The formation of peperites, which occurred by the interaction of lava with wet sediment, is a vitally significant environmental indicator. Nonetheless, few examples of this phenomenon have been comparatively documented, which happened during Archean successions (Beresford, et al., 2002; Wilson and Grant, 2006; Moulton, et al., 2011; Barnes and Van Kranendonk, 2014; Barnes and Arndt, 2019); Proterozoic succession (McPhie, 1993; Rawlings, 1993; Biske, Romashkin and Rychanchik, 2004; Sinha, et al., 2011; Constenius, et al., 2017); Palaeozoic succession (Brooks, 1995; Doyle, 2000; Cas, et al., 2001; Chen, et al., 2013; Zhu, et al., 2014; Chen, et al., 2016; Memtimin, et al., 2020; Bann, Jones and Graham, 2022); Mesozoic succession (Wilson, 1991; Wilson, 1993; Hanson and Hargrove, 1999; Templeton and Hanson, 2003; Hanson and, Nemeth, Breitkreutz and Wilke, et al., 2004; Palinkaš, et al., 2008; Asvesta and Dimitriadis, 2013; Krobicki, et al., 2019); Cenozoic succession (Erkül, Helvaci and Sözbilir, 2006; Martin and Németh, 2007; Busby, et al., 2008; Haller and Németh, 2009; Nouri, et al., 2017); and to the most recent Pleistocene succession around 43,000-12,400 years ago (Mercurio, 2011). However, it has also been pointed out by (Skilling, et al., 2002) that in ancient deposits, it may be difficult to differentiate fragments obtained from this process from those of tectonic origin. Despite this fact, the presence of peperite in oceanic island arcs may infer the primitive arc settings.

Although according to Jassim and Goff (2006) along Iraqi part of Zagros orogeny, the WVsg comprises from the base: Basal Red Beds, Lower Volcanics consisting of mafic, minor felsic lavas and frequently pillow lavas laterally adjacent to the sedimentary sequence (i.e., volcano-flysch unit), Middle Red Beds (±limestones), Upper Volcanics and finally the Upper Red Beds, peperites were not recorded in any sequences within whole succession of WVSg.

III. Geology of the Studied Area and Field Investigations

Peperites in the studied area are exposed at two locations along Mawat-Shasho road, which lies between longitudes 45° 25’ 21.10” E (PF1) – 45°27’11.21” E (PF2) and latitudes 35° 54’ 16.80” N – 35°55’29.65” N, respectively, and 1–4 Km away from East of Mawat town and 37 km north of Sulaimani city (Figs. 2b, 3-5). Stratigraphically, both sites are within the base of WVsg. The WVsg within the Mawat area covers almost 70 km^2. It is adjacent to the Mawat Ophiolite complex (Fig. 2). Along the Mawat-Shasho road, basaltic intrusions and its intermingling with deep-sea sediments have been observed at different locations in the basal part of the WVsg.

Based on the field investigations, the peperite-bearing successions in both PF1 and PF2 show variation in thickness at different sites and are widespread in the study area along the Mawat-Shasho section (Figs. 3-5). PF are discontinuously exposed on both the eastern and western sides of the Mawat-Shasho section. The distance between these two outcrops is about 6–7 km. PF1 and PF2 exhibit lateral lithological changes involving basaltic lava flows interlayered with deep marine succession involving micritic carbonate rocks occasionally associated with shale (a thrust product of basaltic pillow lava) beds. Two lithofacies types are recognized within peperites in the studied area (PF1 and PF2), both are illustrated in discussion section scenarios. Lithofacies Type 1 (PF1) is made up of coherent basaltic pillow lava that is sandwiched between peperites and micritic limestone rocks (Figs. 3, 4 and 6). While lithofacies 2 (PF2) comprises, coherent massive basalt intercalated with host micritic limestone rocks, closely packed vesicular pillow basalt, and peperites (Figs. 5 and 7). The host rocks for both lithofacies types (PF1 and PF2) are deep marine micritic carbonate rocks rich in planktonic Forams (Figs. 4 and 8).

PF1 in the field is characterized by blocky peperites and vesicular pillowed basaltic intrusions with well-layered, thick, and chocolate-colored micritic limestones. The jigsaw texture in the peperitic rocks is well exposed, especially in PF1 (Fig. 3). Even though PF2 is distinguished by fluidal peperites and vesicular to amygdaloidal pillowed basaltic intrusions with well-layered thick chocolate-colored micritic limestones (Fig. 5). In both PF1 and PF2 basaltic intrusions appear as grayish black having normal to the mega-pillow morphologies based on (Walker, 1992) classification and their rounded vesicles diameter range 1–5 mm are often filled with the secondary minerals such as calcite, chlorite, and quartz. The sedimentary rocks have attitudes of 240°/54°/NW, occur as layers to massive chocolate micritic limestones, and cover more than 30–50 m within PF (Fig. 4). Manganese mineralization is well exposed on the micritic limestones in the form of surficial pods (3–5 cm), small tubes, and dendritic structures within PF1, which may indicate the deposition of micritic limestone within a deep marine environment (Fig. 4).

IV. Sampling and Analytical Techniques

The intensive fieldwork encompasses the meticulous collection of samples for peperites, basaltic rocks, and host micritic carbonate rocks, in addition to the comprehensive examination of the petrological and stratigraphical features of the PF. Almost 35 samples have been taken from PF. All 35 samples were cut for thin sections preparation (15 thin sections of basaltic rocks, 10 thin sections of peperitic rocks,

http://dx.doi.org/10.14500/aro.11363

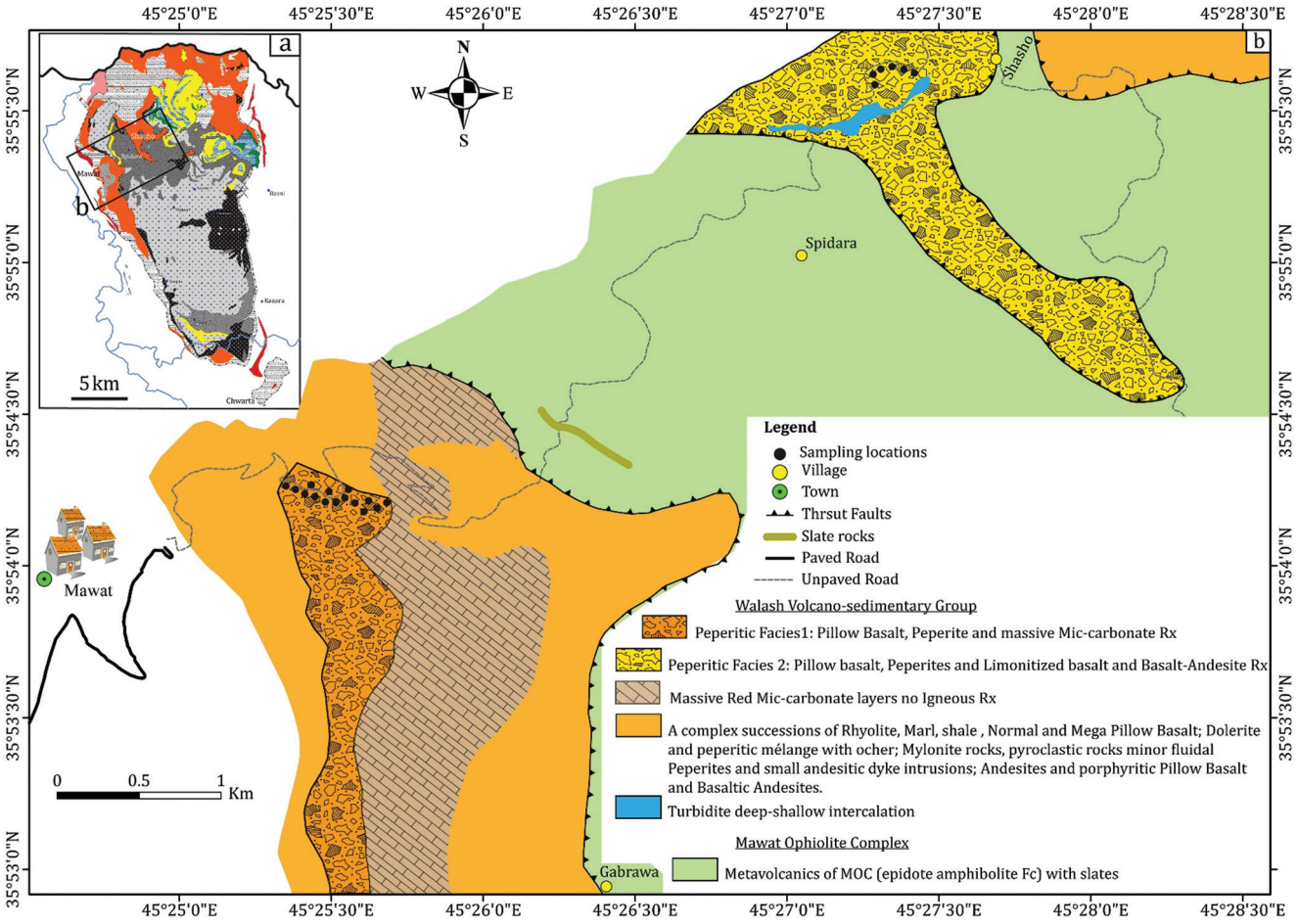

Fig. 2. (a) Location and geological map of the Mawat-Chwarta area of the study area after (Al-Mehaidi, 1974). (b) Detail geological map of the WVsg Mawat-Shasho section.

and 10 thin sections of host micritic carbonate rocks) and for studying their internal structures, textures, mineralogy (modal analysis), and paleontology polarized light microscope were used.

Twenty-six fresh samples have been selected for the mineralogical study. Among them, 20 samples were taken from peperitic rocks (basaltic rocks) and five samples from host micritic carbonate rocks, and one sample from thrust shale which is located between host micritic carbonate rocks and peperitic-basaltic rocks. All samples were grounded into powders for X-ray diffraction analysis at the University of Soran using a Panalytical X'Pert MRD machine. The samples were scanned using a Ni filter and K-Alpha1 radiation (1.54060 Å) at generator settings of 40 mA and 45 kV and recorded diffraction peaks are between 2Θ=5° and 2Θ=70°. Mineral patterns were identified using Match 3 software.

Within (PF1) 10 fresh samples from basaltic rocks and three samples from host micritic carbonate rocks and also 10 fresh samples from basaltic rocks and two samples from host micritic carbonate rocks within (PF2) have been selected for the whole rock geochemistry (major, trace and REE elements) analysis within ALS Laboratories in Seville, Spain.

At the geology department Research Laboratories at the University of Sulaimani, the slabbed whole-rock samples were prepared with a water-cooled diamond-blade saw to remove any weathered or calcified parts of the rock samples. All rock samples were powdered in hardened steel with a chromium-free tool steel vibrating cup mill by using PULVERISETTE 9 machine. Further sample preparations, such as pulverizing to get particle size <75 µm and lithium borate fusion before acid dissolution, have been done at ALS Labs. Whole-rock powders were analyzed by inductively coupled plasma-atomic emission spectroscopy (ICP) and Mass spectrometer (ICP-MS) methods for major, trace, and rare earth element (REE) abundances in the ALS laboratories using geochemical procedures (ME-ICP06; ME-MS81; ME-4ACD81). For major and trace element analyses, structural water was removed from sample powders by heating in a furnace at 1000°C for 30 min. Loss on ignition (LOI) was determined from 1 g of the powdered samples by heating in a furnace at 1000°C, and then the total weight change of the sample powder is calculated. Detection limits are <0.01% for major elements and 0.01–1 ppm for trace and REE elements, except for As and Cr, which have relative errors of 5 ppm. Mg numbers are calculated using the formula Mg# = (100* MgO/[MgO+Fe_2O_3] [molar]). Eu anomalies (Eu/Eu*) have been calculated as Eu/Eu* = (Eu)cn/[(Sm)cn x (Gd)cn]0.5 after McLennan (1989). The Chemical Index of Alterations

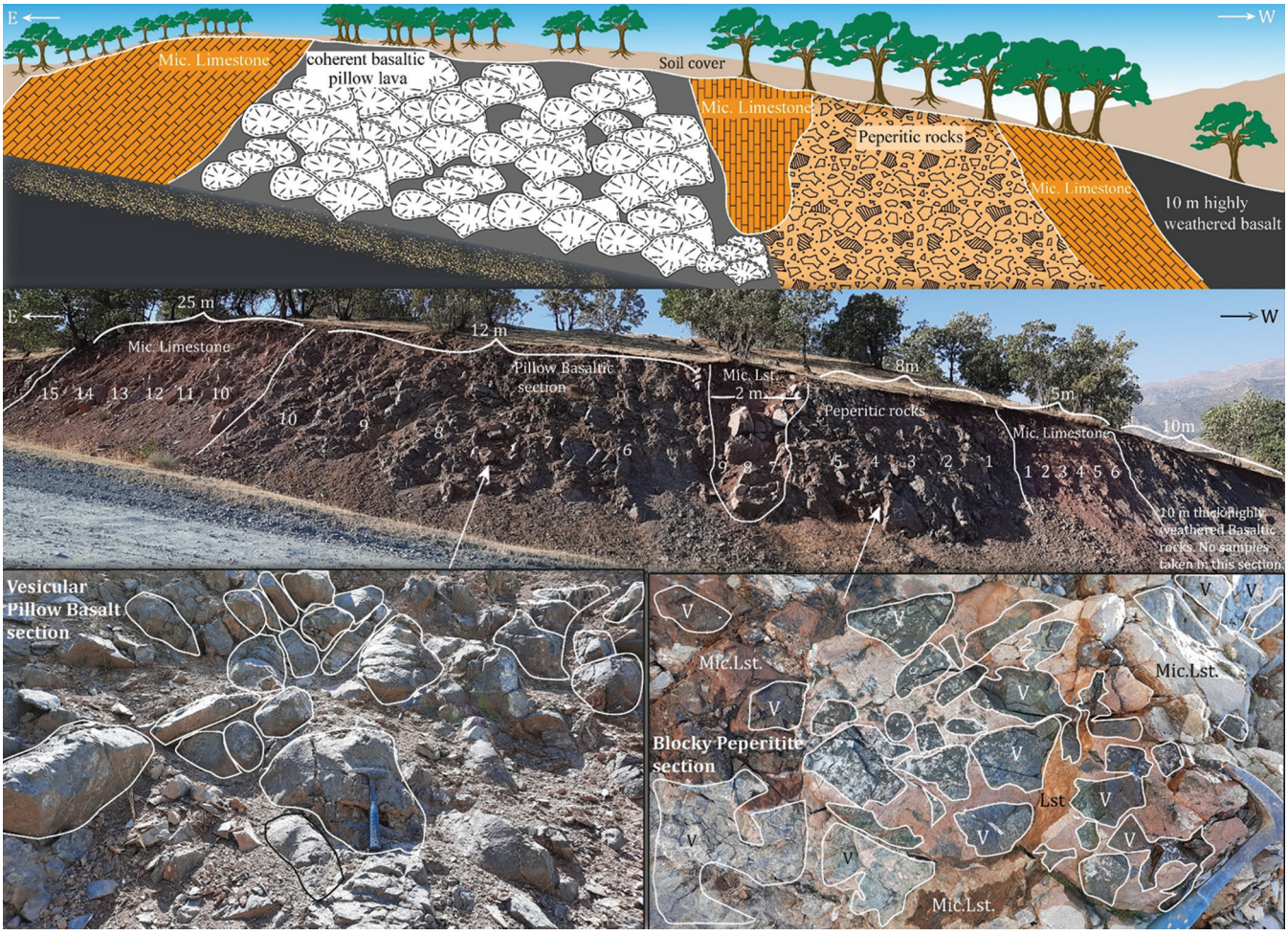

Fig. 3. Panoramic view and illustration of the PF1 outcrop within the Mawat area, comprising intercalation of the basaltic pillow with micritic limestone thick layers, blocky peperites, and coherent basaltic pillow lava. Numbers refer to the sampling locations.

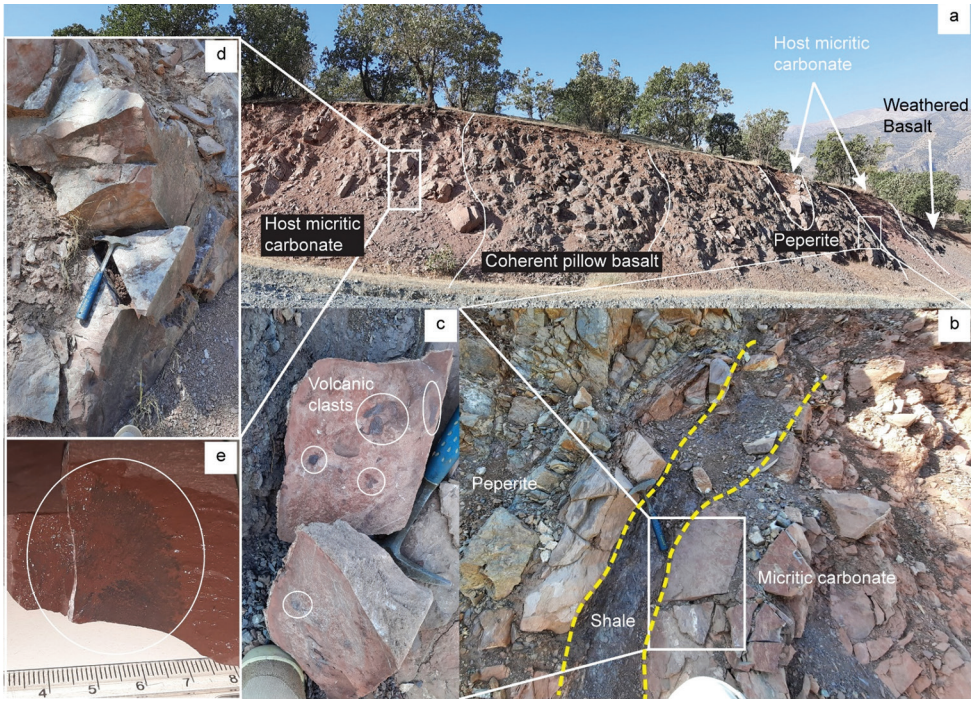

Fig. 4. (a) Panoramic view (~70 m horizontal) of the PF1 outcrop. (b) Shale (thrust) contact between peperite and host micritic carbonate rocks. (c) Centimetric pods of volcanic clasts (white circles) within micritic carbonate rocks. (d) Reddish brown host micritic carbonate rocks. (e) Dendritic structures of manganese mineralization within host micritic carbonate rocks.

http://dx.doi.org/10.14500/aro.11363

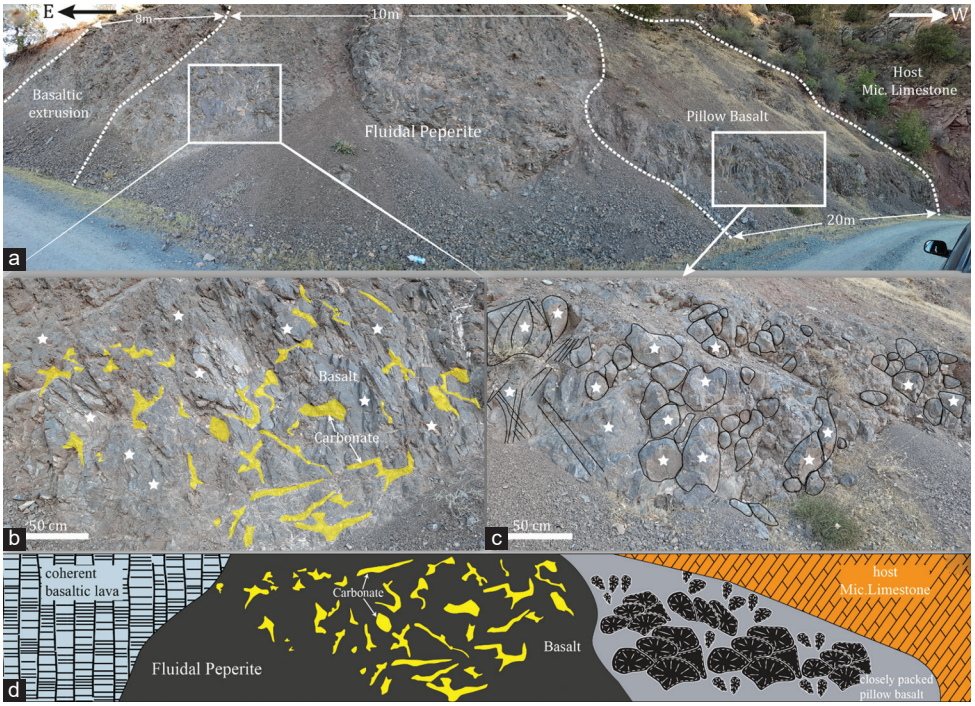

Fig. 5. (a) Panoramic view of the PF2 outcrop near Shasho village. (b) Fluidal peperites. (c) Vesicular pillow basalt outcrop, white stars represent sampling locations. (d) Representative illustration for fluidal peperite outcrop of panoramic view (a). White stars represent sampling locations.

(CIA%) is also calculated using the formula CIA%= 100 * m. Al_2O_3/(m. Al_2O_3+ m. CaO+ m. Na_2O+ m. K_2O) after Nesbitt and Young (1982).

V. Results

A. Petrography

Petrographically, both PF1 and PF2 are composed primarily of plagioclase (45–50%) and clinopyroxene (20–25%) phenocrysts, set in an aphanitic groundmass of the same minerals and associated with hematite (10%) and orthoclase (8%), nepheline and sphene as accessory phases. Although PF1 and PF2 mineralogically are the same, they are showing different textures. PF1 samples tend to be more aphanitic in textures and are characterized by the presence of tachylite, in which skeletal grains of plagioclase (only the outer rim) set in the glassy groundmass (Fig. 9a). PF2 samples indicate more evolved magma and are characterized by porphyritic textures (Fig. 9c-f) in which boxy cellular plagioclase serves an initial mixing stage of magma. It indicates the typical volcanic texture of these rocks (Hibbard, 1995) and references therein (Fig. 9c and d). Amygdaloidal textures are clearly seen in both PF, vesicles are of circular and amoeboid forms and filled with secondary minerals, such as hematite, calcite, and dolomite. This might indicate hydrothermal alterations or submarine weathering in these volcanic rocks (Thompson, 1991) (Fig. 9a, b and e). Pyroxenes in PF1 samples are extremely altered while in PF2 samples, they are less altered (Fig. 9a and e). Despite the submarine hydrothermal alteration, the basaltic rocks in both PF1 and PF2 maintained their original igneous textures such as interstitial, glomerophyric, and intersertal textures.

B. Mineralogy

Detailed mineralogical studies for the PF1, PF2, and host micritic limestone are shown in Table I. XRD analysis shows that the basaltic pillow lavas from PF1 and PF2 comprise major phases, such as albite, andesine, and diopside. While the minor phases comprise hematite, ilmenite, and titanite (Table I). As well as host micritic limestone rocks comprising calcite as major phases and quartz as minor. A 20cm shale in PF1 (thrust product) is between peperites and host micritic limestone rocks. It comprises montmorillonite, quartz, calcite, and anorthite as major phases and pyroxene as minor phases.

C. Geochemistry

Within the studied area, 20 volcanic and five micritic limestones (host) rock representative samples from PF1 and PF2 were analyzed for geochemical classification and interpretation of the peperitic rock types. The major, trace, and REE concentrations of these volcanic and micritic limestone rocks in the PF are given in Tables II and III. Micritic limestone host rocks are characterized by a narrow range in SiO_2 (10.75–11.65 wt.%) and high contents of CaO (45.3–46.7 wt.%) with LOI (36.0–36.8 wt.%). While the concentrations of Al_2O_3, Fe_2O_3, MgO, Na_2O, and K_2O are around 6 wt.%. The geochemical signature of these micritic limestone rocks indicates that the host carbonate rocks in both PF1 and PF2 are deposited in a deep-marine environment.

Meanwhile, the volcanic rock samples in both PF1 and PF2 occupy a narrow range of SiO_2 (43.63–47.57wt.%), Al_2O_3 (16.05–17.85 wt.%), and Fe_2O_3 (10.15–11.35 wt.%.) with relatively high Na_2O and CaO and low K_2O. Furthermore, the amounts of Cr_2O_3, MnO, P_2O_5, SrO, and BaO are <0.5 wt.%. Almost all samples are influenced by

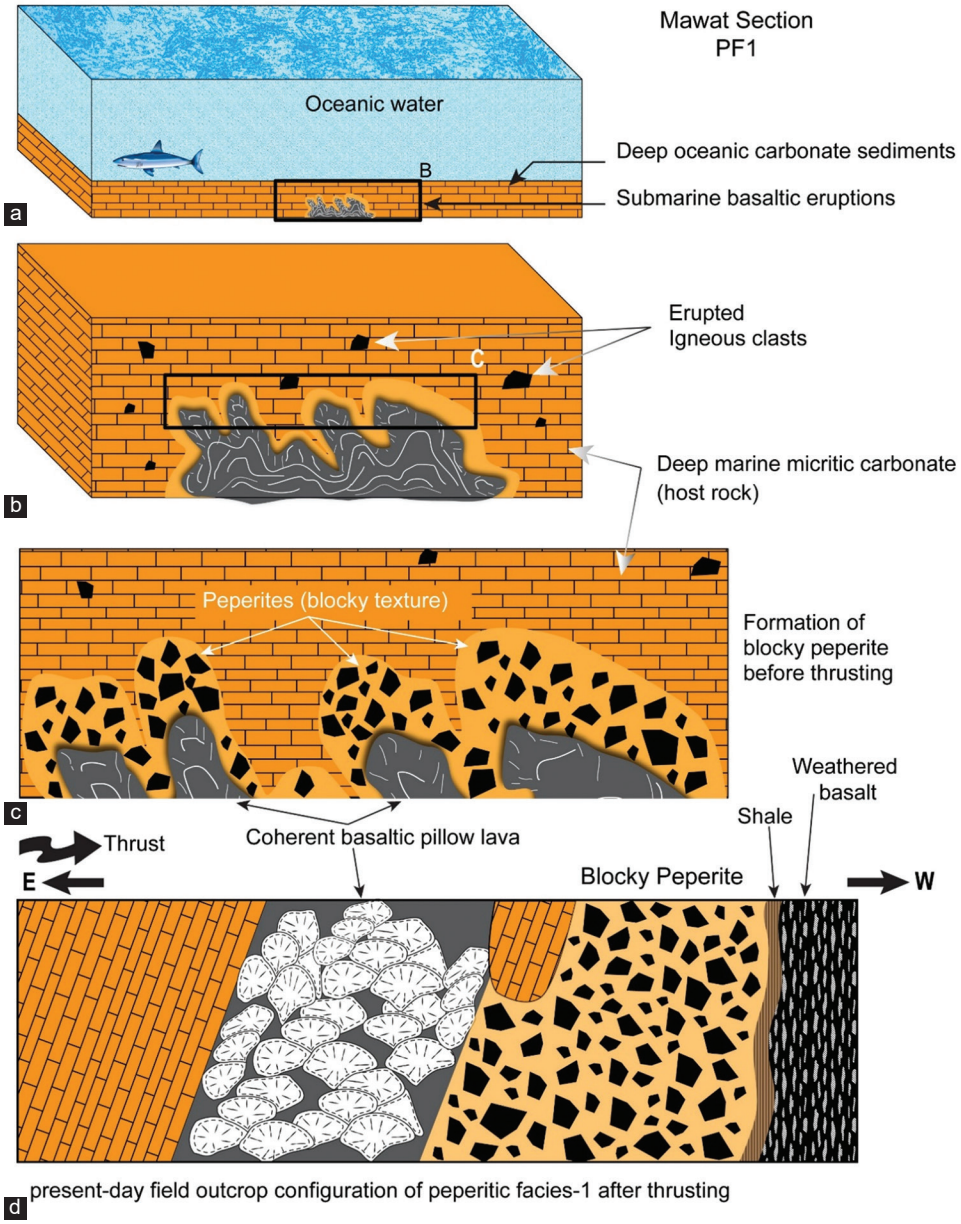

Fig. 6. (a-d) Scenario 1 for the formation of blocky peperite within PF1 (Mawat section).

hydrothermal alteration (Fig. 9a-f). The alteration effects on the volcanic rocks are consistent with the high value of LOI (7.0–9.46%) and the high ratio of alkalies (Na_2O+K_2O).

The use of Harker diagrams reveals a discernible negative or positive correlation between the majority of major oxides and the increasing SiO_2 content. The observed correlations indicate the significant influence of fractional crystallization processes in the development of volcanic rocks within PF 1 and 2. The observed patterns in the concentrations of Al_2O_3, CaO, Na_2O, TiO_2, and Fe_2O_3 relative to SiO_2 indicate a potential process of fractionation involving diopside, plagioclase, sphene, and other iron-titanium oxides, as illustrated in (Fig. 10).

The low concentration of MgO observed in both sections PF1 and PF2 may be attributed to the absence of olivine and amphibole (specifically, Mg-hornblende). Besides, low TiO_2 concentrations of around 1% may reflect the eruption of basaltic submarine eruptions near frontal arc settings (Shuto, et al., 2015). Conversely, the greater concentrations of Fe_2O_3, as indicated by the elevated modal percentage of hematite, are evident in both PF1 and PF2.

The concentrations of trace elements, specifically Nb, Ta, and Ti, exhibit a distinct depletion characteristic in volcanic rocks found in PF1 and PF2. This depletion feature is believed to be an inherent characteristic of the source region of the island arc (Ryerson and Watson, 1987). Furthermore, the concentrations of compatible trace elements, such as chromium (Cr) and nickel (Ni), in the volcanic samples from PF1 and PF2 exhibit a range of (205–380 ppm) and (82–171 ppm), respectively (Tables II and III). As reported by (Humphris and Thompson, 1978), the observed values generally align with the Cr and Ni concentrations found in

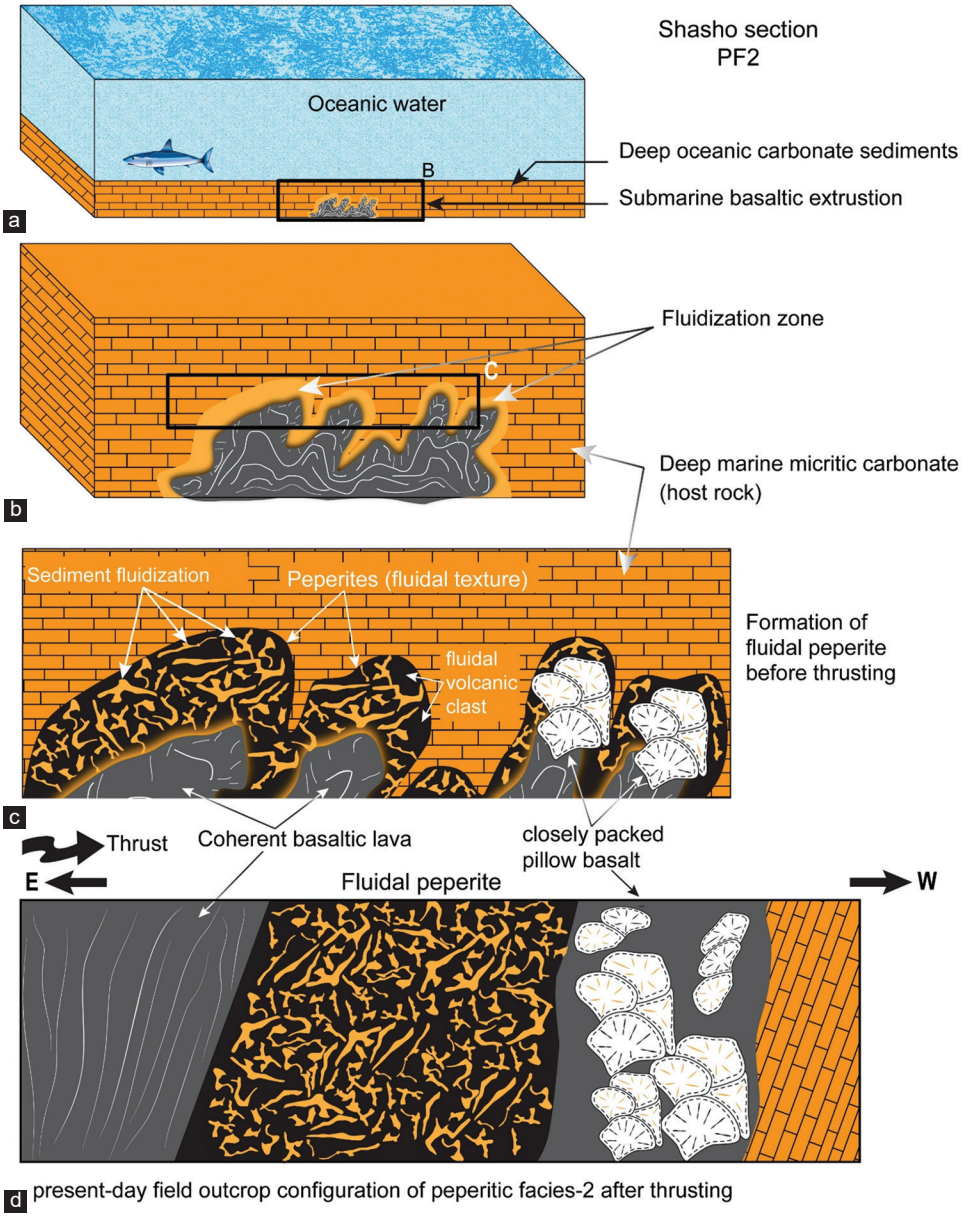

Fig. 7. (a-d) Scenario 2 for the formation of fluidal peperite within PF2 (Shasho section).

fresh basalt, which typically, fall within the range of 280–550 ppm and 75–140 ppm, respectively.

Zirconium (Zr) concentration serves as a reliable indicator of geochemical diversity, functioning as an independent index. It demonstrates a strong correlation with various other elements, thereby enabling the assessment of their mobility (Pearce, et al., 1992; Liu, et al., 2012; Wang, et al., 2016). Therefore, the utilization of Zr as a fractionation index allows for the identification of mafic fractionation processes involving pyroxene and/or olivine, as evidenced by the observed decrease in Cr and Ni (Fig. 11). The presence of a positive correlation between Zr and Y, as well as Zr and Nb, in conjunction with the presence of Ce, may suggest the absence of amphibole and monazite minerals. In general, there is a notable correlation between Zr and REEs (La, Ce, Nd, and Sm), which serves to confirm the immobile nature of these elements during hydrothermal or secondary alteration processes within PF1 and PF2 rock samples (Fig. 11).

All samples, that were plotted on the diagram (Zr/TiO_2–Nb/Y) after (Pearce, 1996), are in the basaltic field and show sub-alkaline characteristics (Fig. 12a). The magmatic nature classification diagrams, after (Miyashiro, 1974) and (Ross and Bédard, 2009), show all samples in the field of tholeiitic nature (Fig. 12b and c). All basaltic rock samples within both PF are characterized by the following elemental ratios: low Nb/Y (0.10-0.15), La/Yb (1.4–2.3), and Nb/La (0.61–0.77); adequately high Zr/Nb (23–30), Hf/Ta (12–22) and Th/Ta (2–5); relatively low contents of major elements, such as TiO_2 and P_2O_5 in contrast to the high ratios of FeO_t/MgO (Tables II and III). Furthermore, on well-known tectonic diagrams, such as Th/Yb versus Ta/Yb after (Pearce, 1982), Ce-Sr-Sm normalized ternary after (Ikeda, 1990), and

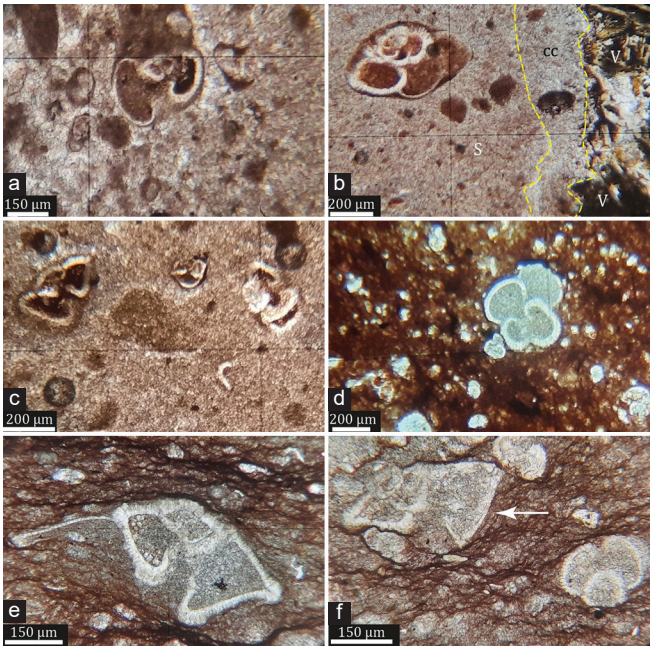

Fig. 8. (a) *Acarinina nitida,* (b) *Morozovella praeangulata,* (c) *Morozovell subbotinae* (left up), *Morozovella apanthesma* (right up), (d) *Morozovella aequa,* (e) *Morozovella velascoensis,* (f) *Morozovella subbotina* (with arrow), *Acarinina soldadoensis* (bottom right). Figures (a-c) are for PF rocks and (d-f) are for host micritic carbonate rocks (S). Volcanic rocks (V), calcite vein represented by cc.

Zr-Ti-Sr ternary after (Pearce and Cann, 1973), these basaltic rocks are plotted in the fields of volcanic arc basalt and island arc tholeiitic basalt, respectively (Fig. 13a-c). Based on the primitive mantle-normalized multielement spider diagram (Fig. 14a), the basaltic rocks in both PF1 and PF2 show selective enrichment in Large-Ion Lithophile Elements (LILEs) (e.g., Rb, Ba, and K) and depletion in the High Field Strength Elements (HFSEs) (e.g., Ta, Nb, Nd, and Ti). It compared with the field of island arc basalts (IAB) after (Perfit, et al., 1980). While on the REE chondrite-normalized diagram (Fig. 14b), these basaltic rocks are characterized by slight enrichment and with flat REE patterns. It compared with the average composition of IAB after (Elliott, 2003) and Izu-Bonin-Mariana arc basalts (IBM Arc) field after (Elliott, et al., 1997).

D. Paleontological Investigation

The authors concentrated on whole PF1 sections for paleontological investigations because the PF1 consists of well crops out of micritic carbonate sequences that sandwiched peperitic rocks in the area (Figs. 3 and 4). The distinguishable facies throughout peperites within WVSg indicated deep marine environments that lack benthonic foraminifera in contrast with the high percentage of planktonic foraminifera, especially *Morozovella* and *Acarinina* which they reflect the deep marine environment

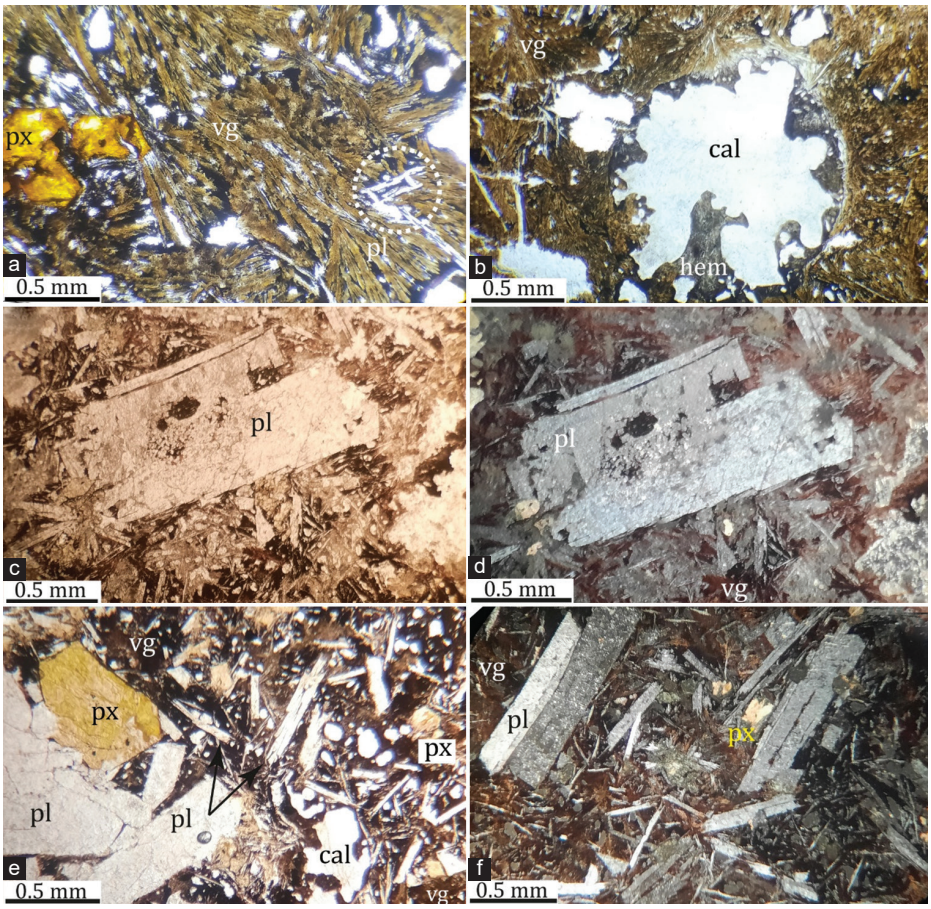

Fig. 9. (a) Tachylite, skeletal plagioclase (pl) with extremely altered pyroxene (px) and volcanic glass (vg) groundmass in PF1 (sample JB1). (b) Amygdule filled with hematite (hem) and calcite (cal) (sample JB6). (c and d) Boxy cellular plagioclase in PF2 (sample JB16). (e and f) Porphyritic basalt in PF2 (sample JB20). Mineral abbreviations after (Whitney and Evans, 2010). Photomicrographs of a, b, c, and e are PPL view; d and f are XPL view.

 http://dx.doi.org/10.14500/aro.11363

TABLE I
XRD Mineralogy (Major & Minor Phases) within PF1 and PF2 and Host Micritic Carbonate Rocks (Mc). (Bst.) Stands for Basalt

Sample	Location	Field description	Major minerals	Minor minerals	Sections
JB1	Mawat	Basaltic-Peperitic rocks contacted with host micritic carbonate rocks	Diopside and Albite	Sodalite and Hematite	
JB2	Mawat	Basaltic-Peperitic rocks 50 cm away from host micritic carbonate rocks	Albite, Andesine and Diopside	Calcite and Hematite	
JB3	Mawat	Fresh pillowed basalt 10m away from Peperitic rocks	Albite, Augite and Anorthite	Hematite	
JB4	Mawat	Fresh pillowed basalt 12m away from Peperitic rocks	Albite, Andesine and Hematite	Calcite and Ilmenite	
JB5	Mawat	Fresh pillowed basalt contacted with host micritic carbonate rock	Albite, Calcite and Ilmenite	Hematite	
JB6	Mawat	Fresh pillowed basalt 12.5m away from Peperitic rocks	Albite, Augite and Ilmenite	Calcite and Hematite	
JB7	Mawat	Fresh pillowed basalt 13m away from Peperitic rocks	Albite, Andesine, Augite and Ilmenite	Calcite and Hematite	
JB8	Mawat	Fresh pillowed basalt 14m away from Peperitic rocks	Albite, Andesine and Ilmenite	Calcite and Hematite	
JB9	Mawat	Fresh pillowed basalt 15m away from Peperitic rocks	Albite, Andesine, Augite and Ilmenite	Calcite and Hematite	
JB10	Mawat	Fresh pillowed basalt 16m away from Peperitic rocks	Albite, Diopside, Anorthite and Ilmenite	Hematite	
JB11	Mawat	Host Micritic carbonate rock, Right side of peperitic rocks	Calcite	Colusite and Quartz	
JB12	Mawat	Host Micritic carbonate rock, Left side of peperitic rocks	Calcite	Quartz	
JB13	Mawat	Host Micritic carbonate rock, Left side of peperitic rocks	Calcite	Quartz	
Shale	Mawat	20 cm Thick Shale rock contacted with samples 1MP and 1MPF	Montmorillonite, Quartz, Calcite and Anorthite	Pyroxene	
JB14	Shasho	Vesicular- amygdaloidal basalt- Peperite	Albite and Diopside	Ilmenite and Hematite	
JB15	Shasho	Vesicular- amygdaloidal basalt- Peperite	Albite and Diopside	Ilmenite and Hematite	
JB16	Shasho	Vesicular- amygdaloidal basalt- Peperite	Albite and Diopside	Ilmenite and Hematite	
JB17	Shasho	Vesicular- amygdaloidal basalt- Peperite	Albite and Diopside	Ilmenite and Hematite	
JB18	Shasho	Vesicular- amygdaloidal basalt- Peperite	Albite and Diopside	Ilmenite and Hematite	
JB19	Shasho	Vesicular- amygdaloidal basalt- Peperite	Albite and Diopside	Titanite and Ilmenite	
JB20	Shasho	Vesicular- amygdaloidal basalt- Peperite	Albite and Diopside	Titanite and Ilmenite	
JB21	Shasho	Vesicular- amygdaloidal basalt- Peperite	Albite and Diopside	Titanite and Ilmenite	
JB22	Shasho	Vesicular- amygdaloidal basalt- Peperite	Albite and Diopside	Titanite and Ilmenite	
JB23	Shasho	Vesicular- amygdaloidal basalt- Peperite	Albite and Diopside	Titanite and Ilmenite	
JB24	Shasho	Micritic carbonate rock, within peperitic rocks	Calcite	Quartz and Colusite	
JB25	Shasho	Micritic carbonate rock, within peperitic rocks	Calcite	Quartz	

TABLE II
Whole-Rock Major, Trace, and REE Concentrations (ICP-MS) of PF1 Rock Samples in the Mawat Area

Peperitic Facies	PF1																		
Sample number	JB1	JB2	JB3	JB4	JB5	JB6	JB7	JB8	JB9	JB10	D.L.	Average	STDEV.	JB11	JB12	JB13	D.L.	Average	STDEV.
Rock type	Basalt	Basalt	Basalt	Basalt	Basalt	Basalt	Basalt	Basalt	Basalt	Basalt		Mean	Precision	Mic. Lst.	Mic. Lst.	Mic. Lst.		Mean	Precision
Oxides (Wt.%)																			
SiO2	47.57	46.11	43.87	45.74	43.99	43.63	46.45	46.00	46.50	46.20	<0.01	45.61	1.32	11.50	11.60	11.65	<0.01	11.58	0.08
Al2O3	16.80	16.40	17.85	17.15	16.05	17.25	17.10	17.00	17.20	17.15	<0.01	17.00	0.49	3.06	3.08	3.07	<0.01	3.07	0.01
Fe2O3	10.40	10.60	11.35	10.95	10.15	10.20	10.95	10.90	10.92	10.85	<0.01	10.73	0.38	1.62	1.68	1.64	<0.01	1.65	0.03
CaO	11.00	12.90	11.10	13.35	13.75	14.70	11.80	11.60	11.70	11.50	<0.01	12.34	1.26	46.40	46.50	46.70	<0.01	46.53	0.15
MgO	3.45	4.46	3.33	2.65	3.04	1.82	3.61	3.50	3.45	3.40	<0.01	3.27	0.68	1.00	1.08	1.06	<0.01	1.05	0.04
Na2O	4.75	4.06	3.62	3.67	3.97	3.65	4.09	4.00	4.05	4.00	<0.01	3.99	0.33	0.34	0.36	0.35	<0.01	0.35	0.01
K2O	0.94	0.48	1.38	1.44	0.85	1.35	1.05	1.00	0.95	0.98	<0.01	1.04	0.29	0.62	0.61	0.62	<0.01	0.62	0.01
Cr2O3	0.05	0.04	0.04	0.04	0.04	0.04	0.04	0.04	0.05	0.04	<0.01	0.04	0.01	0.01	0.01	0.01	<0.01	0.01	0.00
TiO2	1.04	1.08	1.13	1.24	1.08	1.04	1.20	1.10	1.20	1.15	<0.01	1.13	0.07	0.15	0.17	0.16	<0.01	0.16	0.01
MnO	0.17	0.15	0.16	0.16	0.16	0.15	0.18	0.17	0.15	0.16	<0.01	0.16	0.01	0.10	0.10	0.10	<0.01	0.10	0.00
P2O5	0.15	0.10	0.25	0.66	0.33	0.59	0.21	0.40	0.55	0.50	<0.01	0.37	0.20	0.20	0.20	0.21	<0.01	0.20	0.01
SrO	0.07	0.07	0.05	0.06	0.05	0.06	0.07	0.06	0.07	0.07	<0.01	0.06	0.01	0.02	0.02	0.02	<0.01	0.02	0.00
BaO	0.02	0.02	0.03	0.02	0.02	0.03	0.03	0.02	0.03	0.03	<0.01	0.03	0.01	0.01	0.01	0.01	<0.01	0.01	0.00
LOI	7.31	7.44	8.74	7.15	8.45	9.46	7.04	7.10	7.00	7.05	<0.01	7.67	0.88	36.70	36.50	36.00	<0.01	36.40	0.36
TOTAL	103.72	103.92	102.90	104.27	101.92	103.97	103.82	102.89	103.82	103.08		103.43		101.73	101.92	101.60		101.75	
Mg#	58.82	63.58	55.94	52.63	59.70	48.08	58.82	57.14	58.82	52.63		56.62		-	-	-			
CIA%	35.56	34.04	40.00	34.69	33.33	34.00	36.96	37.78	36.96	37.78		36.11		-	-	-			
Trace (ppm)																			
Ag	0.5	0.5	0.5	0.5	0.5	0.5	0.5	0.5	0.5	0.5	0.01-1	0.50	0.00	0.4	0.4	0.5	0.01-1	0.43	0.06
As	5	5	12	27	20	25	19	13	15	22	5	16.30	7.67	9	9	9	5	9.00	0.00
Cd	0.5	0.5	0.5	0.5	0.5	0.5	0.5	0.5	0.5	0.5	0.01-1	0.50	0.00	0.6	0.6	0.6	0.01-1	0.60	0.00

(Contd...)

TABLE II
(Continued)

Peperitic Facies	PF1																		
Sample number	JB1	JB2	JB3	JB4	JB5	JB6	JB7	JB8	JB9	JB10	D.L.	Average	STDEV.	JB11	JB12	JB13	D.L.	Average	STDEV.
Rock type	Basalt	Basalt	Basalt	Basalt	Basalt	Basalt	Basalt	Basalt	Basalt	Basalt		Mean	Precision	Mic. Lst.	Mic. Lst.	Mic. Lst.		Mean	Precision
Co	48	51	54	53	49	45	44	43	46	49	0.01-1	48.20	3.74	7	7	7.2	0.01-1	7.07	0.12
Cu	87	53	133	39	28	27	38	35	44	51	0.01-1	53.50	32.80	31	31	30	0.01-1	30.67	0.58
Li	40	40	40	20	20	10	30	40	38	35	0.01-1	31.30	10.91	10	10	10	0.01-1	10.00	0.00
Mo	1	1	1	1	1	1	1	1	1	1	0.01-1	1.00	0.00	2	1	2	0.01-1	1.67	0.58
Ni	150	160	171	106	121	142	119	120	125	130	0.01-1	134.40	20.64	71	72	71	0.01-1	71.33	0.58
Pb	2	3	2	3	2	4	2	3	2	3	0.01-1	2.60	0.70	4	4	4	0.01-1	4.00	0.00
Sc	35	36	36	40	35	32	37	35	36	35	0.01-1	35.70	2.00	4	4	4	0.01-1	4.00	0.00
Tl	10	10	10	10	10	10	10	10	10	10	0.01-1	10.00	0.00	10	9	10	0.01-1	9.67	0.58
Zn	85	79	115	115	106	104	101	100	105	102	0.01-1	101.20	11.47	30	30	30	0.01-1	30.00	0.00
Ba	203	125	215	149.5	120	204	246	225	240	235	0.01-1	196.25	47.43	126	126.5	127	0.01-1	126.50	0.50
Ce	9.5	9.6	11	13.6	12.2	11.5	14.3	11.2	13.5	12.4	0.01-1	11.88	1.63	10.9	10.8	10.9	0.01-1	10.87	0.06
Cr	380	300	270	240	250	230	230	260	280	265	5	270.50	44.38	51	50	50.5	5	50.50	0.50
Cs	0.72	0.44	1.01	0.94	0.38	1.04	0.86	0.7	0.9	0.85	0.01-1	0.78	0.23	1.15	1.14	1.15	0.01-1	1.15	0.01
Dy	4.09	4.28	4.37	5.32	4.38	3.89	4.74	4.2	4.7	4.5	0.01-1	4.45	0.40	2.38	2.39	2.36	0.01-1	2.38	0.02
Er	2.58	2.87	2.96	3.38	2.99	2.68	3.02	2.7	3	2.95	0.01-1	2.91	0.23	1.43	1.45	1.44	0.01-1	1.44	0.01
Eu	1	0.96	1.09	1.26	1.1	1.04	1.1	1	1.1	1.05	0.01-1	1.07	0.08	0.57	0.59	0.57	0.01-1	0.58	0.01
Ga	15.6	17.2	17.2	17.3	16.1	17.6	17.6	16	17.5	17	0.01-1	16.91	0.73	4.5	4.4	4.6	0.01-1	4.50	0.10
Gd	3.51	3.56	4.03	4.46	3.84	3.78	4.24	3.86	4.2	4	0.01-1	3.95	0.30	2.62	2.62	2.61	0.01-1	2.62	0.01
Hf	1.9	1.9	2	2.2	1.9	2.1	2.4	2	2.3	2.1	0.01-1	2.08	0.18	0.7	0.7	0.7	0.01-1	0.70	0.00
Ho	0.86	0.95	0.97	1.14	0.95	0.92	0.97	0.88	0.98	0.9	0.01-1	0.95	0.08	0.48	0.48	0.49	0.01-1	0.48	0.01
La	3.6	3.8	4.1	5.9	4.8	4.8	6	4.2	5.4	4.9	0.01-1	4.75	0.84	14.6	14.7	14.5	0.01-1	14.60	0.10
Lu	0.38	0.4	0.45	0.53	0.44	0.43	0.46	0.41	0.47	0.45	0.01-1	0.44	0.04	0.18	0.19	0.18	0.01-1	0.18	0.01
Nb	2.4	2.6	2.6	3.6	3.1	3.1	3.6	3.2	3.5	2.3	0.01-1	3.00	0.49	2.6	2.7	2.6	0.01-1	2.63	0.06
Nd	7.9	8.3	8.5	10.6	9.6	9.2	11.2	8.8	10.5	9.8	0.01-1	9.44	1.09	11.4	11.3	11.4	0.01-1	11.37	0.06
Pr	1.54	1.57	1.66	2.18	1.84	1.78	2.11	1.7	2.1	1.9	0.01-1	1.84	0.23	2.64	2.66	2.65	0.01-1	2.65	0.01
Rb	15.4	7.3	22.2	17.8	11.6	16.8	15	15.5	18	16	0.01-1	15.56	3.96	15	15	15	0.01-1	15.00	0.00
Sm	2.59	2.55	2.64	3.37	2.74	2.77	3.05	2.6	3	2.8	0.01-1	2.81	0.26	2.08	2.07	2.08	0.01-1	2.08	0.01
Sn	1	1	1	1	1	1	1	1	1	1	0.01-1	1.00	0.00	1	1	1	0.01-1	1.00	0.00
Sr	705	667	538	556	467	577	651	670	700	680	0.01-1	621.10	80.94	252	250	253	0.01-1	251.67	1.53
Ta	0.1	0.1	0.1	0.1	0.1	0.1	0.2	0.1	0.2	0.1	0.01-1	0.12	0.04	0.2	0.2	0.2	0.01-1	0.20	0.00
Tb	0.62	0.66	0.7	0.78	0.62	0.66	0.72	0.67	0.71	0.69	0.01-1	0.68	0.05	0.37	0.37	0.38	0.01-1	0.37	0.01
Th	0.34	0.4	0.38	0.48	0.41	0.41	0.52	0.44	0.5	0.47	0.01-1	0.44	0.06	1.4	1.3	1.4	0.01-1	1.37	0.06
Tm	0.39	0.42	0.43	0.5	0.41	0.37	0.46	0.42	0.48	0.46	0.01-1	0.43	0.04	0.17	0.17	0.16	0.01-1	0.17	0.01
U	0.28	0.21	0.36	0.32	0.24	0.38	0.26	0.3	0.36	0.33	0.01-1	0.30	0.06	0.24	0.24	0.23	0.01-1	0.24	0.01
V	220	208	219	218	206	218	219	218	222	220	0.01-1	216.80	5.33	17	16	17	0.01-1	16.67	0.58
W	1	1	1	1	1	1	1	1	1	1	0.01-1	1.00	0.00	1	1	1	0.01-1	1.00	0.00
Y	26	25.4	25.3	30.1	26	25.9	27.8	26.5	28	27	0.01-1	26.80	1.48	16.6	16.6	16.7	0.01-1	16.63	0.06
Yb	2.42	2.68	2.85	3.18	2.9	2.64	2.59	2.67	2.8	2.7	0.01-1	2.74	0.21	1.22	1.21	1.23	0.01-1	1.22	0.01
Zr	72	74	75	93	84	79	100	85	95	90	0.01-1	84.70	9.66	27	28	26	0.01-1	27.00	1.00
Eu/Eu*	1.02	0.98	1.03	1	1.04	0.99	0.94	0.97	0.95	0.97				-	-	-			
(La/Sm)N	0.76	0.82	0.85	0.96	0.96	0.95	1.08	0.89	0.99	0.96				-	-	-			
(La/Yb)N	0.9	0.86	0.87	1.12	1	1.1	1.4	0.95	1.17	1.1				-	-	-			
(Tb/Yb)N	1.09	1.05	1.05	1.04	0.91	1.06	1.18	1.07	1.08	1.09				-	-	-			

Mic Lst.: Micritic Limestone, D.L.: Detection Limit, STDEV.:Standard Deviations

with tropical to subtropical climate condition (BouDagher-Fadel, 2015).

Ten samples were dated using planktonic foraminifera, five samples were from peperitic rocks taken from the contact of basaltic-carbonate clasts (blocky peperites). The other five samples were taken from host micritic carbonate rocks. Both of these section samples gave us the same planktonic foram species (Figs. 8 and 15). The systematic investigation of planktonic foraminifera enabled us to identify 13 species and subspecies in the studied sections (Fig. 8) including *Morozovella praeangulata; Morozovella apanthesma*; *Morozovella angulata*; *Morozovella subbotinae; Morozovella accuta*; *Morozovella occlusal*; *Morozovella cf. apanthesma*; *Morozovella velascoensis*; *Morozovella aequa*; *Acarinina nitida*; *Acarinina soldadoensis*; *Subbotina cancellate;* and *Globanomalina chapmani*. To recognize these species, a lot of sources were used including (Cushman, 1925; White, 1928; Parr, 1938; Morozova, 1939; Toulmin, 1941; Cushman, 1942; Martin, 1943; Bronnimann, 1952; Loeblich Jr. and Tappan, 1957; Blow, 1979; Olsson, et al., 1999; Berggren, et al., 2006). The stratigraphic distribution of these planktonic foraminiferal assemblages permits the recognition of 15 biozones, two dominant biozones (P3 and P4) after (Wade, et al., 2011) have established in WVSg (Middle Paleocene). The

 http://dx.doi.org/10.14500/aro.11363

TABLE III
WHOLE-ROCK MAJOR, TRACE, AND REE CONCENTRATIONS (ICP-MS) OF PF2 ROCK SAMPLES IN THE MAWAT AREA

Peperitic Facies	PF2																	
Sample number	JB14	JB15	JB16	JB17	JB18	JB19	JB20	JB21	JB22	JB23	D.L.	Average	STDEV.	JB24	JB25	D.L.	Average	STDEV.
Rock type	Basalt	Basalt	Basalt	Basalt	Basalt	Basalt	Basalt	Basalt	Basalt	Basalt		Mean	Precision	Mic. Lst.	Mic. Lst.		Mean	Precision
Oxides (Wt.%)																		
SiO2	44.56	45.96	46.22	45.30	45.80	46.10	46.25	45.71	45.84	45.50	<0.01	45.72	0.51	10.75	10.80	<0.01	10.78	0.04
Al2O3	16.40	16.80	16.60	16.90	17.00	17.11	17.20	17.05	17.08	16.95	<0.01	16.91	0.25	2.90	2.95	<0.01	2.93	0.04
Fe2O3	10.55	10.58	10.50	10.52	10.60	10.90	10.95	10.91	10.93	10.58	<0.01	10.70	0.19	1.74	1.73	<0.01	1.74	0.01
CaO	12.20	12.00	12.10	12.00	12.40	12.10	11.70	12.15	11.92	12.02	<0.01	12.06	0.18	45.70	45.30	<0.01	45.50	0.28
MgO	3.29	3.25	3.28	3.21	3.22	3.20	3.20	3.23	3.24	3.27	<0.01	3.24	0.03	1.63	1.60	<0.01	1.62	0.02
Na2O	3.64	3.62	3.60	3.70	3.80	3.86	3.88	3.75	3.82	3.72	<0.01	3.74	0.10	0.20	0.25	<0.01	0.23	0.04
K2O	1.28	1.26	1.25	1.22	1.08	1.02	0.99	1.10	1.05	1.20	<0.01	1.15	0.11	0.61	0.60	<0.01	0.61	0.01
Cr2O3	0.03	0.03	0.04	0.04	0.04	0.04	0.04	0.04	0.04	0.04	<0.01	0.03	0.00	0.01	0.01	<0.01	0.01	0.00
TiO2	1.15	1.16	1.17	1.14	1.60	1.17	1.18	1.50	1.16	1.15	<0.01	1.24	0.17	0.15	0.17	<0.01	0.16	0.01
MnO	0.15	0.15	0.16	0.15	0.16	0.16	0.17	0.16	0.16	0.15	<0.01	0.16	0.01	0.05	0.10	<0.01	0.08	0.04
P2O5	0.16	0.20	0.16	0.19	0.25	0.27	0.30	0.21	0.23	0.20	<0.01	0.22	0.05	0.07	0.10	<0.01	0.09	0.02
SrO	0.04	0.06	0.06	0.06	0.06	0.07	0.07	0.06	0.06	0.06	<0.01	0.06	0.01	0.03	0.02	<0.01	0.03	0.01
BaO	0.02	0.02	0.02	0.02	0.02	0.02	0.02	0.02	0.02	0.02	<0.01	0.02	0.00	0.01	0.01	<0.01	0.01	0.00
LOI	8.74	8.60	8.00	7.70	7.50	7.00	7.00	7.40	7.20	7.10	<0.01	7.62	0.64	36.80	36.50	<0.01	36.65	0.21
TOTAL	102.21	103.69	103.15	102.15	103.53	103.02	102.95	103.29	102.75	101.96		102.87		100.65	100.14		100.40	
Mg#	56.85	58.82	59.70	62.50	54.24	57.43	53.56	58.55	57.72	56.55		57.59		-	-			
CIA%	35.56	36.36	35.56	37.78	36.96	36.96	37.78	36.96	37.78	37.78		36.95		-	-			
Trace (ppm)																		
Ag	0.5	0.5	0.5	0.5	0.5	0.5	0.5	0.5	0.5	0.5	0.01-1	0.50	0.00	0.5	0.5	0.01-1	0.50	0.00
As	12	14	15	17	22	20	21	19	13	15	5	16.80	3.52	5	6	5	5.50	0.71
Cd	0.5	0.5	0.5	0.5	0.5	0.5	0.5	0.5	0.5	0.5	0.01-1	0.50	0.00	0.5	0.6	0.01-1	0.55	0.07
Co	39	38	40	42	41	45	49	48	50	47	0.01-1	43.90	4.43	6	7	0.01-1	6.50	0.71
Cu	79	75	77	80	85	90	88	82	76	87	0.01-1	81.90	5.34	16	17	0.01-1	16.50	0.71
Li	30	32	31	28	35	34	38	33	40	37	0.01-1	33.80	3.77	10	10	0.01-1	10.00	0.00
Mo	1	1	1	1	1	1	1	1	1	1	0.01-1	1.00	0.00	1	1	0.01-1	1.00	0.00
Ni	83	82	84	90	88	85	95	92	100	98	0.01-1	89.70	6.41	70	71	0.01-1	70.50	0.71
Pb	5	4	5	4	3	5	2	4	3	3	0.01-1	3.80	1.03	5	4	0.01-1	4.50	0.71
Sc	33	34	35	36	32	38	40	37	39	38	0.01-1	36.20	2.66	4	4	0.01-1	4.00	0.00
Tl	10	10	10	10	10	10	10	10	10	10	0.01-1	10.00	0.00	10	10	0.01-1	10.00	0.00
Zn	86	86	88	90	98	92	94	103	101	95	0.01-1	93.30	6.02	36	35	0.01-1	35.50	0.71
Ba	138.5	138	139	160	202	223	231	218	220	229	0.01-1	189.85	40.79	47.6	49	0.01-1	48.30	0.99
Ce	12.7	12.5	12.6	12.1	13.2	14	13.8	12.9	13.3	13.5	0.01-1	13.06	0.61	9	10	0.01-1	9.50	0.71
Cr	200	210	205	230	220	260	254	235	249	208	5	227.10	21.82	60	60	5	60.00	0.00
Cs	0.98	0.94	0.98	0.9	0.8	0.85	0.88	0.87	0.95	0.99	0.01-1	0.91	0.06	0.85	0.9	0.01-1	0.88	0.04
Dy	4.19	4.18	4.2	4.23	4.27	4.31	4.39	4.25	4.28	4.33	0.01-1	4.26	0.07	1.83	1.9	0.01-1	1.87	0.05
Er	2.59	2.58	2.6	2.7	3.1	2.85	2.77	2.9	2.65	2.68	0.01-1	2.74	0.17	1.14	1.5	0.01-1	1.32	0.25
Eu	1.15	1.14	1.16	1.12	1.22	1.19	1.18	1.13	1.24	1.23	0.01-1	1.18	0.04	0.43	0.45	0.01-1	0.44	0.01
Ga	17.6	17.5	17.7	17.2	17.9	16.8	16.2	16.6	16.9	16.5	0.01-1	17.09	0.57	3.8	4	0.01-1	3.90	0.14
Gd	3.79	3.77	3.8	3.7	4.1	3.82	3.85	3.78	3.84	3.9	0.01-1	3.84	0.11	1.94	2	0.01-1	1.97	0.04
Hf	2.3	2.2	2.4	2.1	1.95	2.22	2.15	2.19	2.35	2.38	0.01-1	2.22	0.14	0.5	0.6	0.01-1	0.55	0.07
Ho	0.97	0.96	0.98	0.88	0.93	0.95	0.91	0.92	1	0.99	0.01-1	0.95	0.04	0.37	0.38	0.01-1	0.38	0.01
La	4.8	4.7	4.9	4.1	4.5	5	5.2	5.1	4.6	4.3	0.01-1	4.72	0.35	10.7	10.8	0.01-1	10.75	0.07
Lu	0.39	0.38	0.4	0.42	0.44	0.45	0.41	0.37	0.43	0.46	0.01-1	0.42	0.03	0.14	0.15	0.01-1	0.15	0.01
Nb	3.7	3.4	3.5	2.7	2.9	3.1	3.3	3	3.6	2.8	0.01-1	3.20	0.35	2.2	2.3	0.01-1	2.25	0.07
Nd	9.8	9.7	9.9	10.2	8.9	9.2	9.6	9.4	8.6	9.3	0.01-1	9.46	0.48	9.5	10	0.01-1	9.75	0.35
Pr	1.87	1.86	1.88	1.82	1.78	1.75	1.82	1.85	1.89	1.93	0.01-1	1.85	0.05	2.28	2.3	0.01-1	2.29	0.01
Rb	23.6	23.4	23.8	21	18	16	19	21.5	22	22.5	0.01-1	21.08	2.62	19	19	0.01-1	19.00	0.00
Sm	3.01	3.01	3.02	2.6	2.9	2.92	2.68	2.84	2.81	2.77	0.01-1	2.86	0.14	1.96	1.98	0.01-1	1.97	0.01
Sn	1	1	1	1	1	1	1	1	1	1	0.01-1	1.00	0.00	1	1	0.01-1	1.00	0.00
Sr	488	485	489	490	520	510	535	570	512	515	0.01-1	511.40	26.42	319	320	0.01-1	319.50	0.71
Ta	0.2	0.2	0.2	0.2	0.1	0.2	0.1	0.2	0.1	0.2	0.01-1	0.17	0.05	0.1	0.2	0.01-1	0.15	0.07
Tb	0.68	0.66	0.69	0.7	0.65	0.72	0.64	0.73	0.75	0.77	0.01-1	0.70	0.04	0.34	0.35	0.01-1	0.35	0.01
Th	0.41	0.4	0.41	0.42	0.45	0.44	0.38	0.39	0.4	0.46	0.01-1	0.42	0.03	1.48	1.5	0.01-1	1.49	0.01
Tm	0.38	0.36	0.4	0.46	0.42	0.45	0.39	0.37	0.44	0.47	0.01-1	0.41	0.04	0.16	0.16	0.01-1	0.16	0.00
U	0.3	0.29	0.32	0.31	0.33	0.37	0.35	0.39	0.38	0.29	0.01-1	0.33	0.04	0.38	0.35	0.01-1	0.37	0.02
V	223	222	224	225	220	228	227	221	214	215	0.01-1	221.90	4.63	20	19	0.01-1	19.50	0.71

(Contd...)

TABLE III
(Continued)

Peperitic Facies	PF2																	
Sample number	JB14	JB15	JB16	JB17	JB18	JB19	JB20	JB21	JB22	JB23	D.L.	Average	STDEV.	JB24	JB25	D.L.	Average	STDEV.
Rock type	Basalt	Basalt	Basalt	Basalt	Basalt	Basalt	Basalt	Basalt	Basalt	Basalt		Mean	Precision	Mic. Lst.	Mic. Lst.		Mean	Precision
W	1	1	1	1	1	1	1	1	1	1	0.01-1	1.00	0.00	1	1	0.01-1	1.00	0.00
Y	24.5	25	25.5	25.8	26.2	26.9	27.2	26.5	27.6	28.3	0.01-1	26.35	1.19	12.8	13	0.01-1	12.90	0.14
Yb	2.67	2.65	2.68	2.66	2.9	2.73	2.75	2.69	2.82	2.78	0.01-1	2.73	0.08	0.86	0.9	0.01-1	0.88	0.03
Zr	86	84	86	85	87	83	88	82	87	89	0.01-1	85.70	2.21	20	21	0.01-1	20.50	0.71
Eu/Eu*	1.05	1.04	1.05	1.11	1.09	1.1	1.13	1.06	1.16	1.15				-	-			
(La/Sm)N	0.87	0.86	0.89	0.86	0.85	0.94	1.06	0.98	0.9	0.79				-	-			
(La/Yb)N	1.09	1.07	1.11	0.93	0.94	1.11	1.15	1.15	0.99	0.87				-	-			
(Tb/Yb)N	1.08	1.06	1.1	1.12	0.95	1.12	0.99	1.15	1.13	1.18				-	-			

Mic Lst.: Micritic Limestone, D.L.: Detection Limit, STDEV.:Standard Deviations

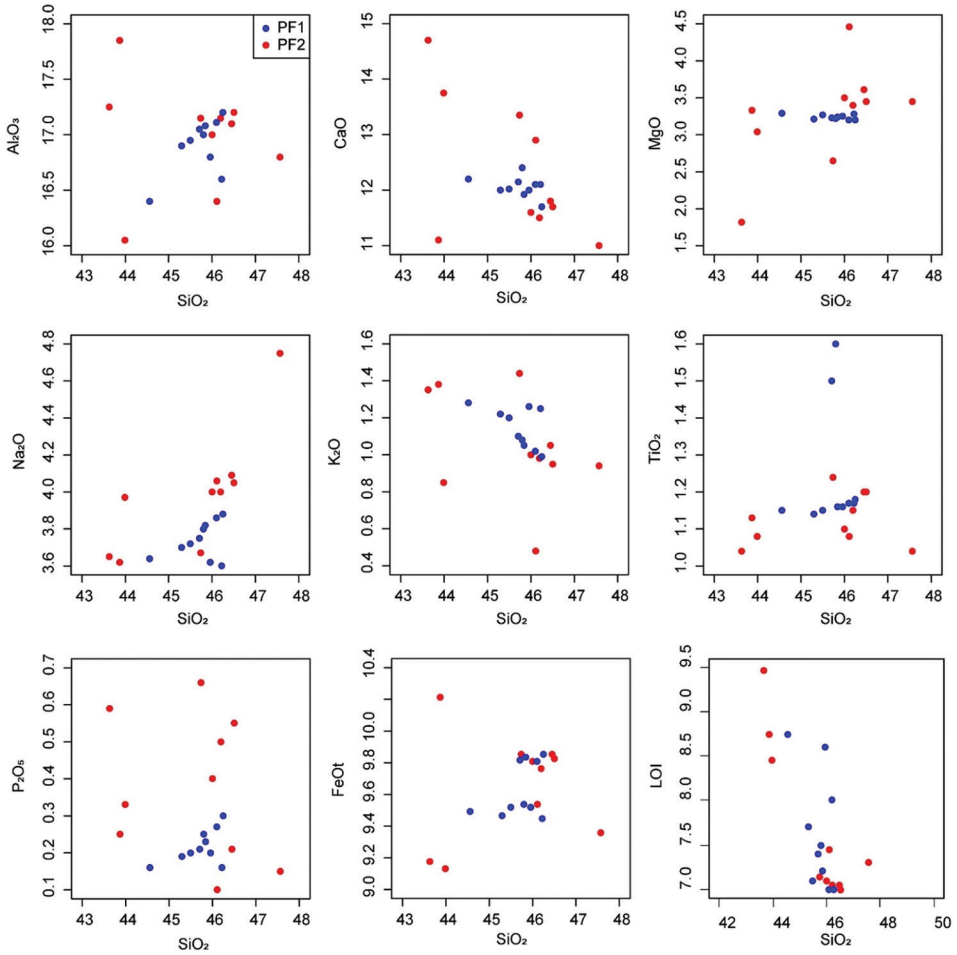

Fig. 10. Harker diagram SiO_2 based versus major elements (Wt.%) for the basaltic rock samples from PF1 and PF2 within WVSg.

peperitic rocks in WVSg were dated to 60 million years ago, corresponding to the Selandian stage of the Middle Paleocene, based on the presence of a *Morozovella* assemblage zone.

VI. Discussion

A. PF in WVSg

As a first attempt, in this paper, two kinds of PF have been recognized in the WVSg. However, to define any PF in any tectonic setting, two principal rules of (White, Mcphie and Skilling, 2000; Skilling, et al., 2002) must be fulfilled: (1) The presence of unconsolidated wet sediment or poorly consolidated sediment; (2) The confirmation of hot magma and its in-situ disintegration and intermingling with the host sediment. Regarding WVSg, the PF1 and PF2 possess the two principal rules as they are clearly seen in the fields. Thus, volcanic rocks and peperites are ubiquitous components within the WVSg of all studied sections in the Mawat area.

http://dx.doi.org/10.14500/aro.11363

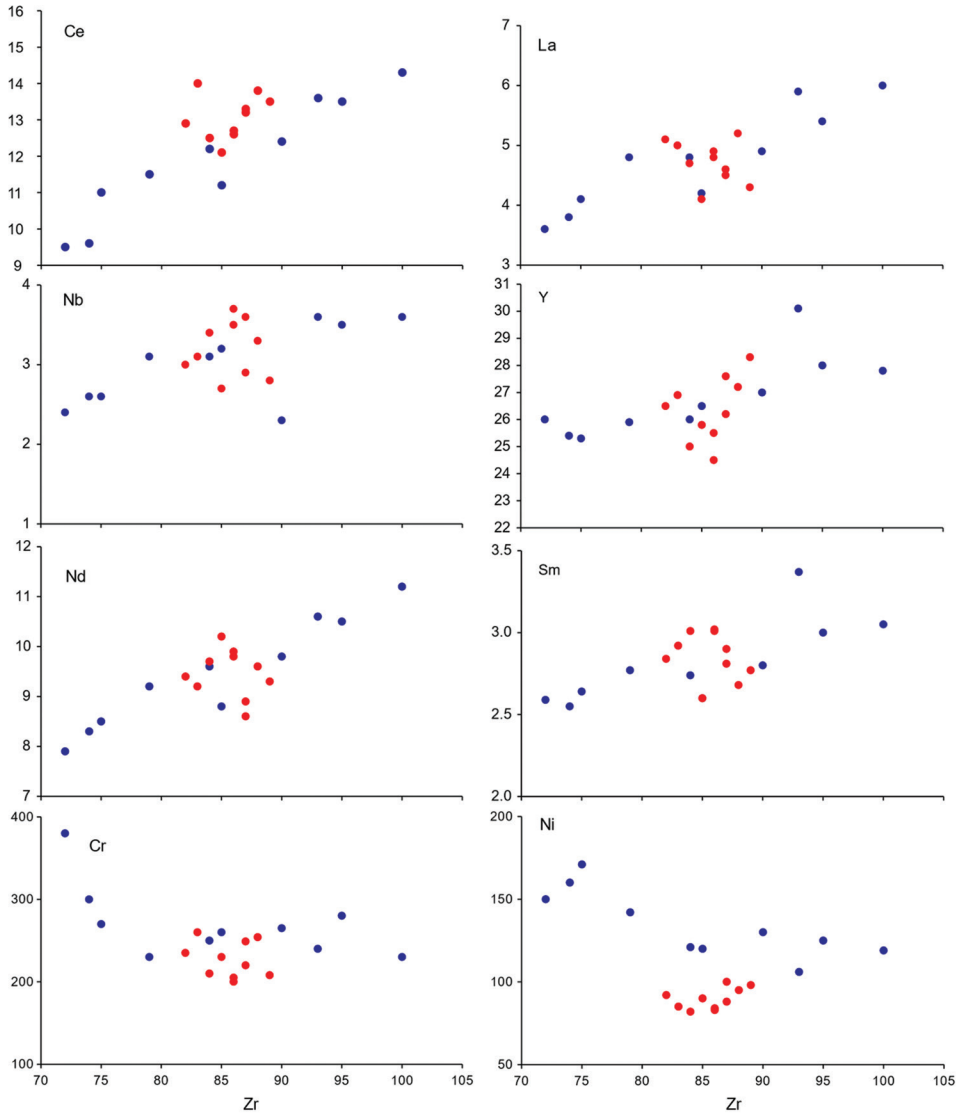

Fig. 11. Binary plots of Zr (ppm) vs selected trace and REE elements (ppm) for the volcanic rocks within PF1 and PF2. Symbols are the same as in Fig. 10.

TABLE IV
WALASH PEPERITE MAJOR-TRACE ELEMENTAL RATIOS COMPARISION TO THE WPB-MORB AND ARCB-NMORB AFTER (CONDIE, 1989).

Major-Trace elemental ratios	WPB-MORB	ARCB-NMORB	Walash Peperite
Nb/La	>1	≤1	0.47-0.77
Hf/Ta	<5	≥5	12-22
Ti/Y	≥350	<350	240-281
Ti/V	>30	≤30	27-31
TiO2%	>1.25	≤1.25	1.04-1.2
Ta(ppm)	>0.7	≤0.7	0.1-0.2
Nb(ppm)	>12	≤12	2.4-3.7

WPB: Within Plate Basalt; MORB: Mid Oceanic Ridge Basalt; NMORB: Normal Mid Oceanic Ridge Basalt; ARCB: Arc Basalt.

TABLE V
WALASH PEPERITE MAJOR-TRACE ELEMENTAL RATIOS COMPARISION TO THE NMORB AND ARCB AFTER (CONDIE, 1989).

Trace elemental ratios	NMORB	ARCB	Walash Peperite
Th/Yb	≤0.1	>0.1	0.13-0.2
Th/Nb	≤0.07	>0.07	0.11-0.2
Nb/La	>0.8	≤0.8	0.47-0.77
Hf/Th	≥8	<8	4.33-5.88

NMORB: Normal Mid Oceanic Ridge Basalt; ARCB: Arc Basalt.

The peperite-bearing successions in WVSg have varying thicknesses at several places across the research area, which includes the PF1 and PF2 study areas (Figs. 3-5). Their deposits are exposed in a discontinuous fashion across the entirety of the Walash volcanic arc basin (Fig. 2b), including both its eastern and western sides of the WVSg. Peperite-bearing successions are often made up of basaltic lava flows that have intruded carbonates and volcaniclastics, as their primary constituents. A deep carbonate sequence has been found in both the eastern and western sides of the PF (Figs. 3-5). This succession displays a lateral lithological change as it moves right and left flanks. In general, both PF 1 and 2 are composed of basaltic lava flows that are interlayered with deep marine-rich planktonic rocks that consist of micritic carbonate horizons.

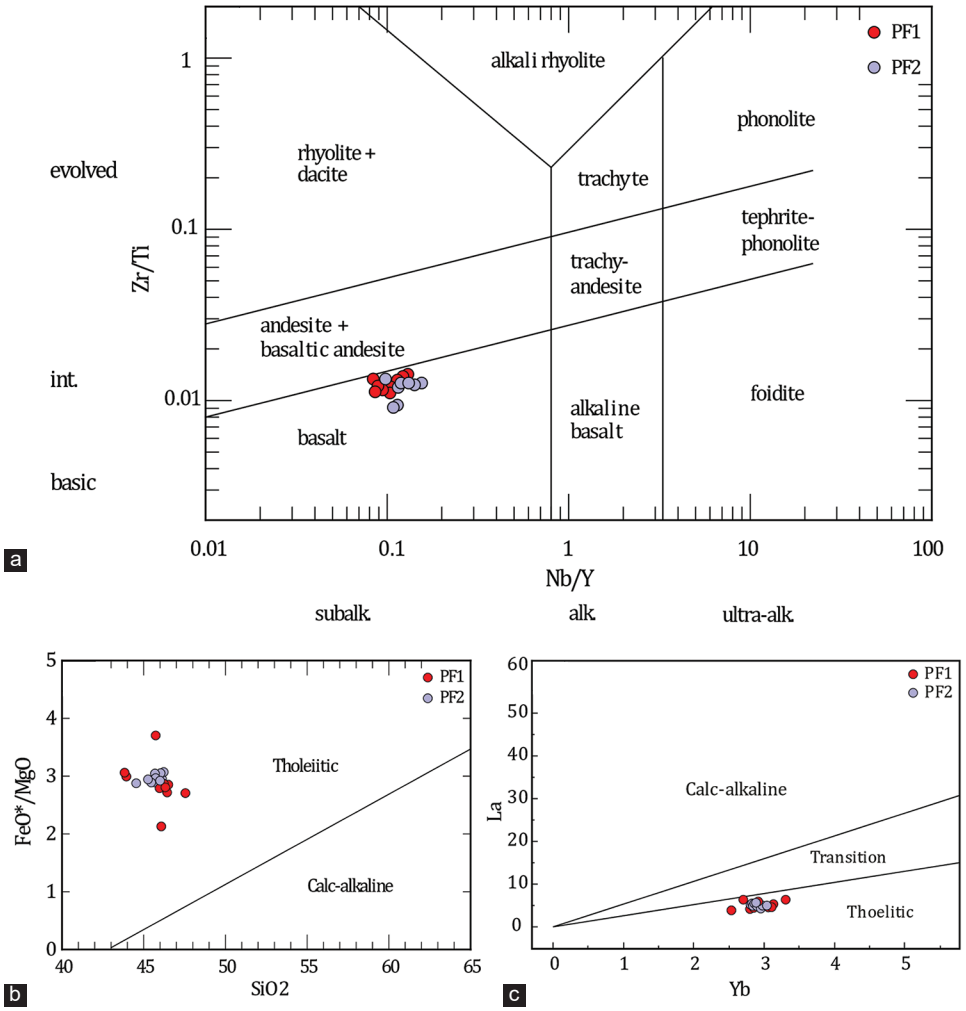

Fig. 12. Rock classification and characteristics of volcanic rocks within PF1 and PF2 (a) Zr/TiO_2 versus Nb/Y of (Pearce, 1996) after (Winchester and Floyd, 1977). (b) SiO_2 versus (FeO_t/MgO) diagram of (Miyashiro, 1974) and (c) La versus Yb after (Ross and Bédard, 2009), showing the tholeiitic nature of the PF1 and PF2 volcanic rocks.

Two types of peperite occur in the Mawat-Shasho area, these include (a) PF1 characterized by blocky peperite related to the rapid submarine eruption of basaltic rocks into wet, unconsolidated deep-marine sediments (host micritic limestone) (Figs. 3, 6, and 9). (b) PF2 is characterized by fluidal peperite associated with the more evolved palagonitized basaltic lava flows into wet, unconsolidated deep-marine sediment (Figs. 5, 7 and 9e, f). Base lithology extension of the Walash arc and PF in the Mawat area was compared with the similar peperites and their extended range from minor occurrences adjacent to igneous extrusions up to deposits with quantities of several km^3 within Mull lava field of NW Scotland by (Brown and Bell, 2007). In this way, the Walash arc base distance may extend to several kilometers based on petrological field evidence.

Accurate and effective volcanic age estimates necessitate a meticulous differentiation between primary and secondary volcanic deposits and volcanosedimentary rocks. Primary volcaniclastic deposits and volcano-sedimentary rocks are non-reworked deposits formed directly from volcanic eruptions (i.e., pyroclastic, autoclastic, hyaloclastic, and peperitic) (White and Houghton, 2006; Sohn and Sohn, 2019). They are distinguished from other volcaniclastic deposits that are not directly related to eruptions but are reworked, modified, and redeposited by surface or gravitational processes (e.g., tides, waves, currents, or non-eruptive gravitational density flows in the oceanic realm) and are classified as epiclastic or secondary (White and Houghton, 2006).

Contemporaneous and non-reworked beds of peperitic rocks have been found throughout the whole section of Mawat-Shasho. According to (Nayudu, 1971), it is conclusive that fossils can be discovered in primary volcaniclastic piles, even in solid basalts. When there is a good record of foraminiferal assemblages with chronostratigraphic value, such as planktonic forams, biochronostratigraphic methods can be used to date volcanic events. Dating peperitic rocks with the presence of short-geologic-range planktonic Foram species, including specifically *Morozovella praeangulata* and *Morozovella angulata* (ranging only 1–2 Ma), is vital and helpful to understand the contemporaneous idea behind the eruption of submarine volcanism into wet, unconsolidated sediments throughout the Walash volcanic area. In this

http://dx.doi.org/10.14500/aro.11363

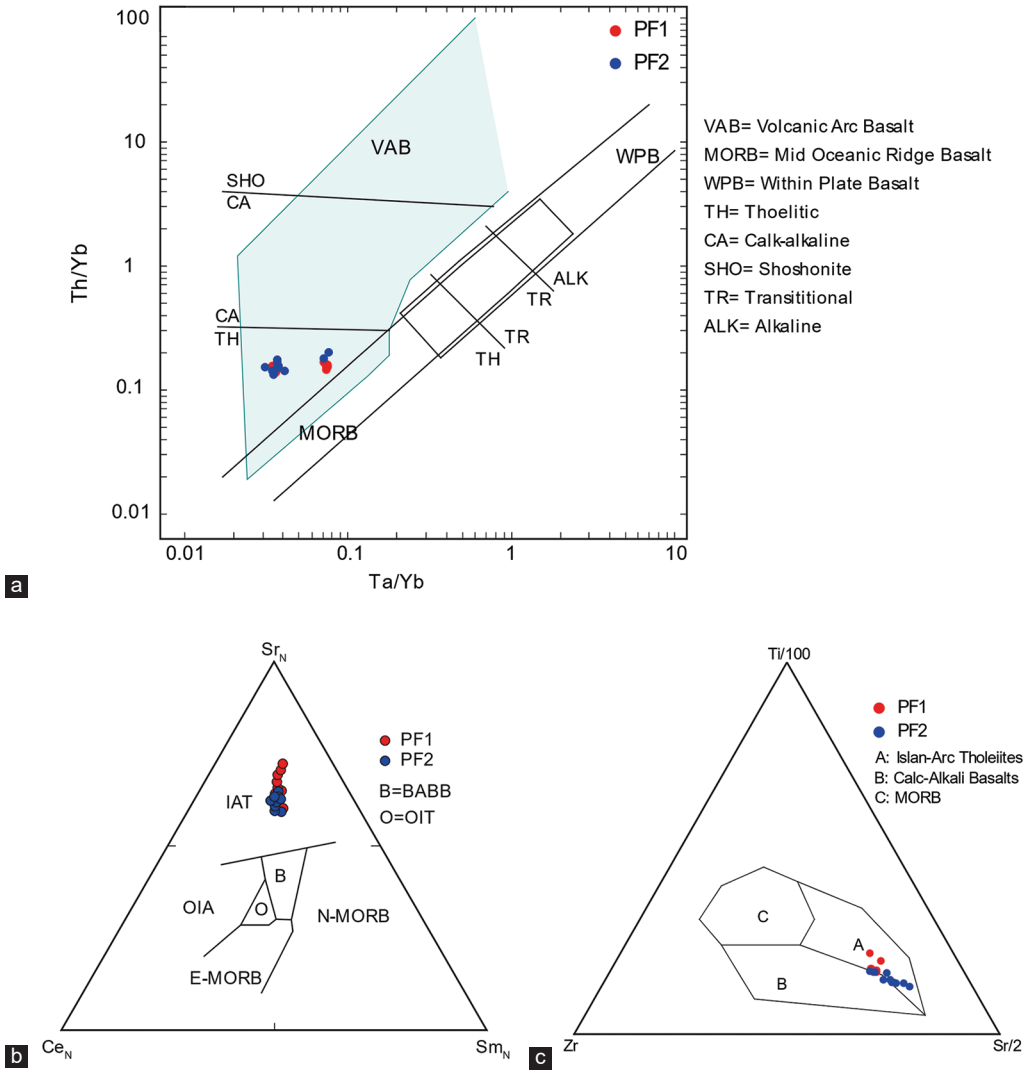

Fig. 13. Tectonic diagrams for PF1 and PF2 Basaltic rocks. (a) Th/Yb versus Ta/Yb after (Pearce, 1982). (b) Ce_N-Sr_N-Sm_N ternary after (Ikeda, 1990) and (c) Zr-Ti-Sr ternary after (Pearce and Cann, 1973).

particular instance, we used planktonic fauna to date volcanic rocks (contemporaneous with the age of deep-marine micritic carbonate rocks) within PF due to the absence of normative zircon and numerous problems within hydrothermally altered volcanic rocks, including grain size and freshness of phenocrysts; whole rock low K content and low K/Ca content; common replacement of crystalline plagioclase and other K-rich phenocrysts. The aforementioned obstacles represent particular difficulties for dating these volcanic rocks using U-Pb and Ar/Ar dating geochronological methods, respectively.

The results indicate that the presence of basaltic rocks, peperites, host micritic carbonate rocks, and shales with some volcaniclastic rocks as well as mélange of mentioned rocks are robust to the presence of a complex primitive volcanic arc in the studied area. Furthermore, because volcanic arcs are large and geologically comprise heterogeneous structures (Stern, 2010), different perspectives of geoscience have been used in this research, such as field investigations, geochemistry, sedimentology, and paleontology. All mentioned tools together will explain the contemporaneity of the basaltic rocks with deep marine sediments in both PF1 and PF2 and based on a precise paleontological study the peperitic rocks dated to the Middle Paleocene, that is, 60 Ma. This age represents the beginning of submarine eruptions in the initial volcanic arc stage within WVSg. These peperites and initial arc volcanic rocks were formed by the subduction of the Arabic Plate beneath the Iranian Plate (Fig. 16).

B. Geochemical Signatures and Tectonic Implications

The peperite concept has changed greatly since its original application, and how and where the peperite form is still a lively topic of debate. The authors precisely prepared volcanic rock samples for geochemical analysis by removing all altered and weathered parts, thus the chemical index of alteration (CIA) value is consistent with fresh basaltic rocks after Nesbitt and Young (1982) and ranging between (33.33–40.0)%. Besides, a minor amount of nepheline in these basaltic rocks may refer to the assimilation of the basic magma with carbonate rocks (Iacono Marziano, et al., 2008), and this will allow the magma to be rich in Na and nepheline

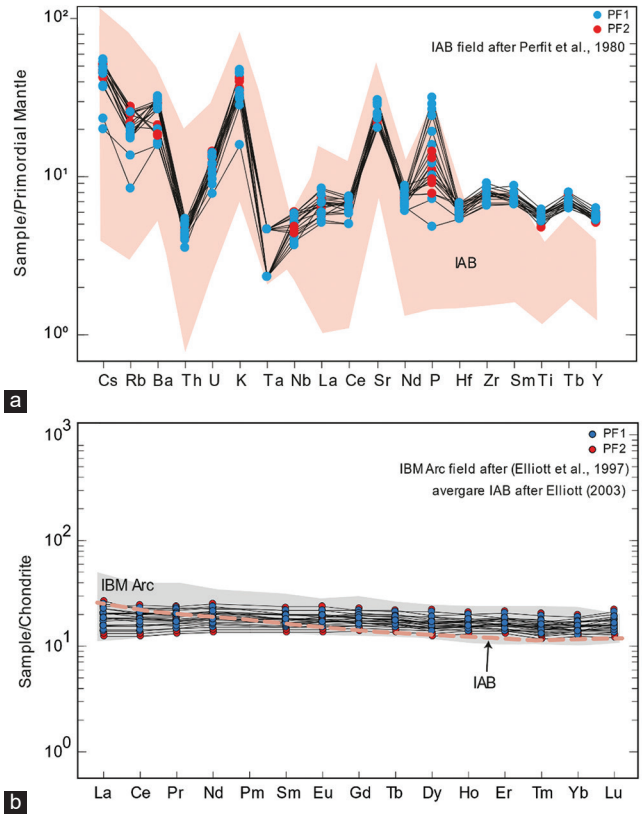

Fig. 14. (a) Multi-element spider diagram normalized to the primordial mantle (normalizing values are from [Wood, et al., 1979] and IAB field after [Perfit, et al., 1980]). (b) Chondrite-normalized REE patterns (normalizing values are from [Sun and McDonough, 1989]) for the basaltic rocks within PF1 and PF2 (average composition of IAB is from [Elliott, 2003], IBM Arc: Izu – Bonin – Mariana arc basalts field after [Elliott, et al., 1997]).

as a minor phase may found in the peperitic rocks despite their tholeiitic nature.

Considering altered arc volcanic rocks, the diagram (Zr/TiO_2-Nb/Y) can be used to replace the total alkali-Silica diagram (Winchester and Floyd, 1977; Pearce, 1996; Hastie, et al., 2007). It is not reasonable to use (Winchester and Floyd, 1977) classification, because it is not robust in classifying altered volcanic rocks (Hastie, et al., 2007). Thus, to determine the classification of mafic volcanic rocks from PF1 and PF2, the data were plotted on a Zr/TiO_2 versus Nb/Y diagram, as shown in Figure 12a. All samples fell within the basaltic field and exhibited sub-alkaline characteristics. Furthermore, their tholeiitic nature is obvious from petrochemical discrimination diagrams of SiO_2 versus (FeO_t/MgO) after Miyashiro (1974) and La versus Yb after Ross and Bédard (2009) (Fig. 12b and c). Basaltic rocks within both PF are characterized by the following elemental ratios: low Nb/Y (0.10-0.15), La/Yb (1.4–2.3), and Nb/La (0.61–0.77); adequately high Zr/Nb (23–30), Hf/Ta (12–22) and Th/Ta (2–5); relatively low contents of major elements like TiO_2 and P_2O_5 (Tables II and III) in contrast to the high ratios of FeO_t/MgO, which are diagnostic features of subalkaline (tholeiitic) rocks in primitive arc basalts (Miyashiro, 1974; Winchester and Floyd, 1977; Condie, 1989; Ross and Bédard, 2009).

Using Condie (1989) basaltic trace elemental ratios, a comparison is made between the Walash peperite and the various types of basalt, such as Within Plate Basalt-Normal Mid Oceanic Ridge Basalt (WPB-NMORB) and Arc Basalt-Normal Mid Oceanic Ridge Basalt (ARCB-NMORB). The trace elemental ratios of Walash peperite are in agreement with those of ARCB and NMORB (Table IV). It should be noted that the ARCB and NMORB are difficult to

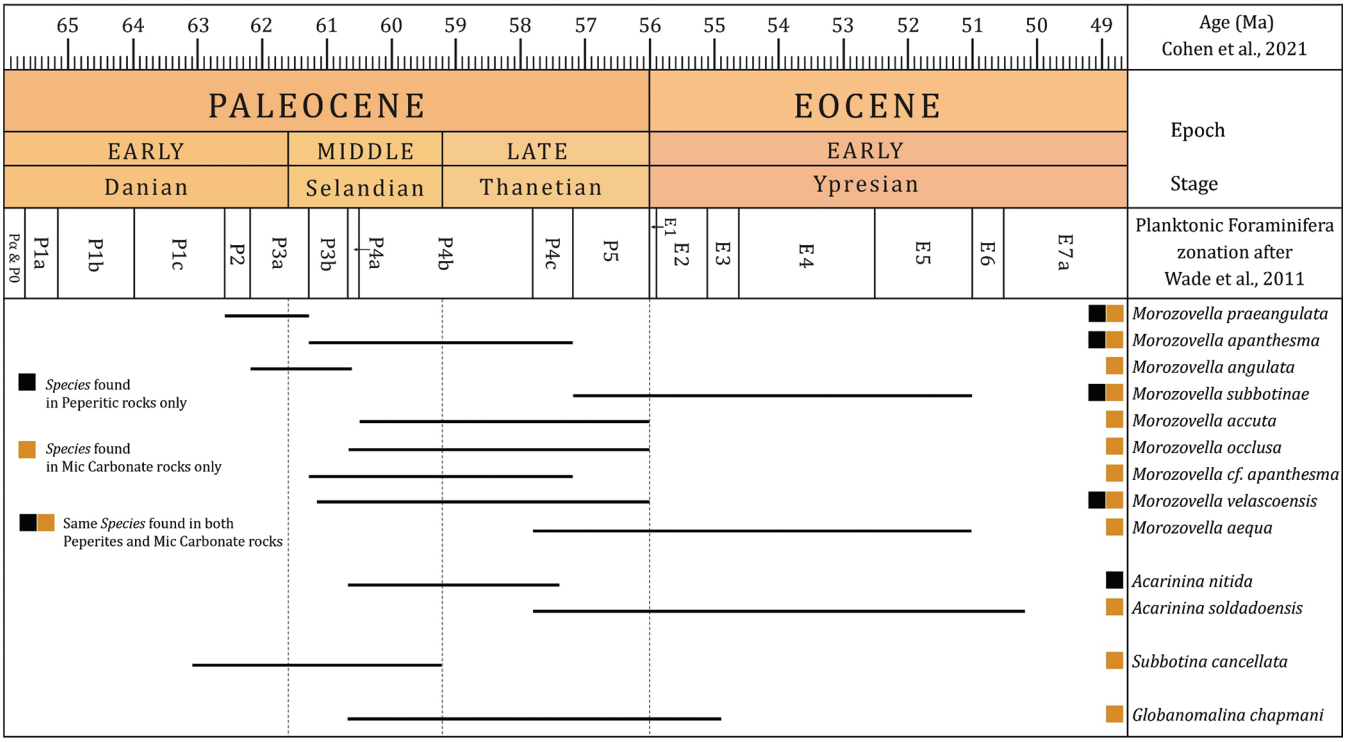

Fig. 15. Biozonation study for Paleocene peperitic rocks (PF1) within WVSg. Ages after (Cohen, et al., 2021

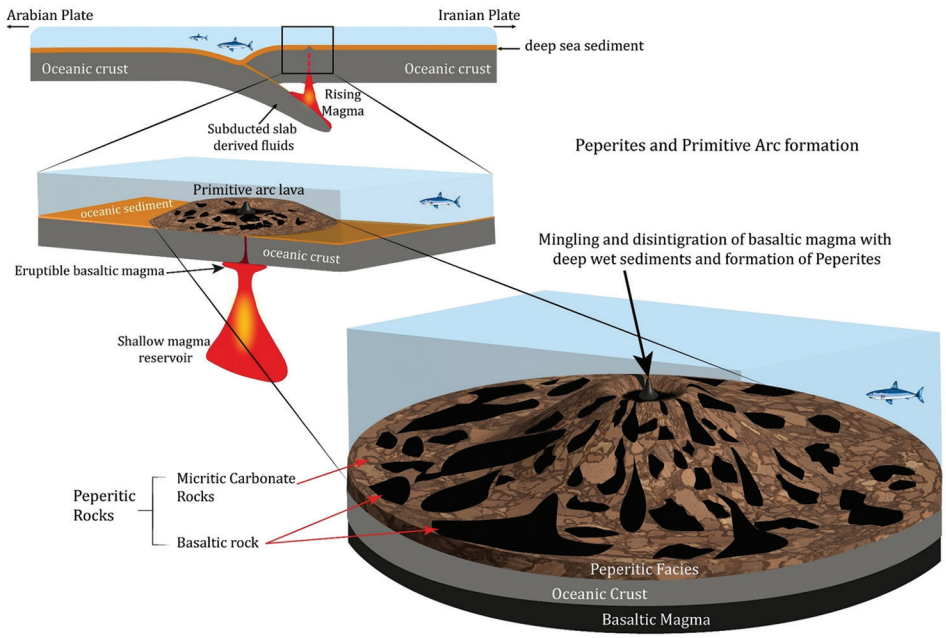

Fig. 16. Generalized tectonic model (not to scale) to illustrate the formation of peperitic facies within the Walash volcano-sedimentary group in the Mawat area in response to the subduction of the Arabian Plate beneath the Iranian Plate in Paleocene (60 Ma).

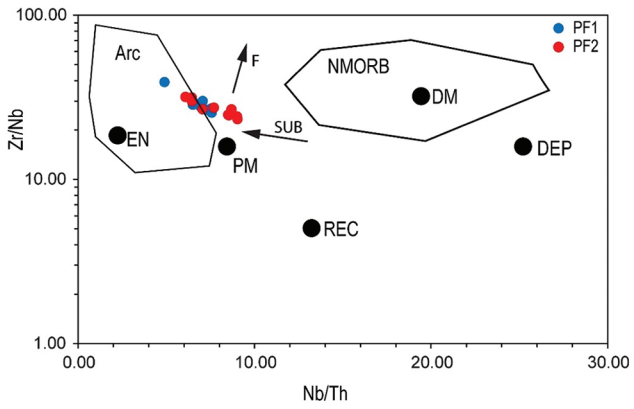

Fig. 17. Nb/Th vs. Zr/Nb elemental ratios for PF1 and PF2 volcanic rock sample, showing samples plotted within the Arc field and their consistent trends with the partial melting subduction-derived fluid trends after Condie (2005). Arrows indicate the effects of batch melting (F) and Subduction-derived fluids. EN: Enriched component; PM: Primitive mantle; DM: Shallow depleted mantle; DEP: Deep depleted mantle; REC: Recycled component; Arc: Arc-related basalts; NMORB: Normal ocean ridge basalt.

differentiate in general; however, using several different ratios of trace elements, such as Th/Yb, Th/Nb, Nb/La, and Hf/Th (Tables IV and V), it is possible to overcome this issue (Condie, 1989).

Using trace elemental ratios, such as Nb/Th and Zr/Nb, the arc basaltic source for Walash peperites can be distinguished from the NMORB basaltic source (Fig. 17). According to (Condie, 2005), arc basalts may have similar Zr/Nb ratios, but they are quite different in Nb/Th ratios. Thus, arc basaltic sources for Walash peperite on an Nb/Th–Zr/Nb plot seem robust. Furthermore, the headed arrows are quite consistent with the Walash volcanic data, which indicate subduction-related derived fluid effects (Condie, 2005).

Based on the primitive mantle-normalized multielement spider diagram (Fig. 14a), the basaltic rocks in both PF1 and PF2 show selective enrichment in LILEs (e.g., Rb, Ba, and K) and depletion in HFSEs (e.g., Ta, Nb, Nd, and Ti) indicate an arc volcanic feature (Saunders and Tarney, 1979) and compared with the field of IAB after (Perfit, et al., 1980). While on the REE chondrite-normalized diagram (Fig. 14b), these basaltic rocks are characterized by slight enrichment and with flat REE patterns which is consistent with the same normalized ratio of (La/Yb) ≈1 for IAB (Perfit, et al., 1980; Philpotts and Ague, 2022). As well as, the absence of the negative Europium (Eu) anomaly suggests that the plagioclase role is insignificant during magma evolution in the area (Slovenec, Lugovic and Vlahovic, 2010; Philpotts and Ague, 2022). Furthermore, in Figure 14a and b, these basaltic rocks were compared and consistent with the average composition of IAB after (Elliott, 2003) and Izu-Bonin-Mariana arc basalts (IBM Arc) field after (Elliott, et al., 1997).

However, PF1 and PF2 basaltic rocks have a geochemical affinity to normal island arcs. In the Sr/Y versus Y diagram (Fig. 18a), basaltic rocks were plotted in the normal island arc magma field suggesting a high concentration of Y with low concentration ratios of Sr/Y. This low ratio of Sr/Y suggests partial melting or fractionation at lower pressure (<≈1 GPa.), in addition, the absence of garnet ± amphibole will cause Y to behave incompatibly, and simultaneously stable plagioclase absorbs Sr as a result, a melt with low Sr/Y will form (Lieu and Stern, 2019). Based on these incompatible trace ratios and tectonic models of Lieu and Stern (2019), we infer that basaltic rocks in the PF1 and PF2 were generated by the partial melting of subducted slabs deep within 30 km and accompanying derived fluids above the subducted slab.

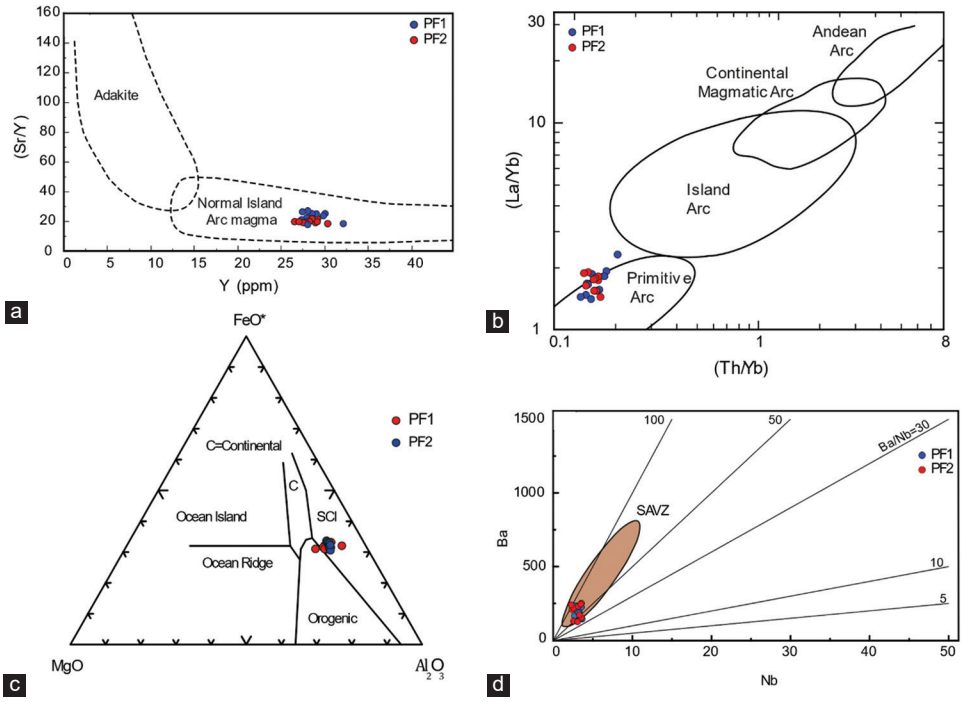

Fig. 18. (a) Sr/Y versus Y diagram showing Island arc magmatic field for the basaltic rocks in PF1 and PF2 after Rogers and Hawkesworth (1989), adakite field is after Defant and Drummond (1990). (b) La/Yb versus Th/Yb tectonic discrimination diagram showing primitive arc setting for basaltic rock samples from the PF1 and PF2 after Condie (1989). (c) FeO-MgO- Al_2O_3 showing Spreading center Island arc (SCI) tectonic setting for PF1 and PF2 basaltic rocks after Pearce, *et al*., 1977. (d) Ba versus Nb diagram for arc front volcanic rocks, (SAVZ) field represents south Andes volcanic rocks after Aragón, et al. (2013).

Furthermore, positive Sr, Ba, and K and negative Nb and Ta anomalies indicate magma generated at the subduction zone (Pearce, 1983). Peperites uniquely suggest a tectonic signature for the submarine eruptions into host sediments. However, their identification indicates contemporaneous magmatism and sedimentation. It helps to reconstruct facies architecture, paleoenvironmental conditions, and tectonic settings. In this circumstance and using available data, the PF1 and PF2 volcanic rocks yielded a primitive arc setting. As well as, their formation in the spreading center of the Island basalts suggest their eruption might happen at the initial arc stage of the volcanic arcs in the arc fronts (Fig. 18b and d), respectively. In addition, the Ba vs. Nb diagram was utilized to confirm the depiction of arc fronts in these PF, and their arc front signatures were compared to those of the South Andes arc front volcanic rocks after (Aragón, et al., 2013) (Fig. 18d). Thus, all geochemical indicators suggest that the PF1 and PF2 should be considered as a part of the subduction zone arc front tectonic settings. Consequently, the authors proposed a tectonic model and two scenarios to illustrate the formation of peperitic rocks in the arc fronts and indicate the submarine eruptions into wet host sediments (Figs. 6, 7, 16). The details of the proposed scenarios for the formation of peperites within WVSg are illustrated in Figures 6 and 7. The first scenario deals with the explosive eruptions of submarine basaltic pillow lava into wet, unconsolidated sediments within the base of the Walash arc (Fig. 6). While the second scenario is represented by the submarine extrusions of massive coherent basalt and closely packed basaltic pillow lava into wet, unconsolidated deep marine carbonate sediments within the base of the Walash arc (Fig. 7).

VII. Conclusions

Peperitic rocks in WVSg are classified into blocky and globular (fluidal) peperitic rocks based on field investigations and textural evidences. In contrast to previous interpretations of the Walash stratigraphy base unit as volcaniclastics, detail mapping and petrological study during this work have revealed a coherent stratigraphy of volcano-sedimentary made up of intrusions of basaltic pillow lavas into micritic carbonate sequence. The newly mapped unit nominated as PF, outcropped in two locations consequently as PF1 and PF2, are texturally classified as blocky and fluidal peperitic rocks, respectively. Volcanic intrusions in the PF classified as basaltic rocks showing tholeiitic magma series based on geochemical signature and positive Sr, Ba, and K and negative Nb and Ta anomalies indicate magma generated at the subduction zone. Dating of the host micritic carbonates and sedimentary clasts in contact with the basaltic rocks within the PF, using planktonic foraminifera, shows that the submarine eruptions occurred during the middle of Paleocene time around 60 Ma and might continue to the 43 Ma which is compatible with the age determined suing Ar-Ar geochronology. Geochemical data suggest these basaltic rocks formed as a result of partial melting of subducting slab under the influence of slab-derived fluids at an approximate depth of 30 km and their eruption into wet sediment also

suggests a spreading center of arc front at the early stage of the Walash volcanic arcs.

In summary, for the first time, we have reported the simultaneous occurrence of basaltic pillow lava and deep-marine micritic carbonate rocks using comprehensive and precise field investigations, petrological, geochemical, and biostratigraphical studies. The identified peperites present within the WVSg indicate simultaneous volcanism and sedimentation and that the Neo-Tethys was still open throughout the Paleocene (~60 Ma).

Acknowledgments

The authors are grateful to Dr. Yadolah Ezampanah from Bu-Ali Sina University (Hamadan, Iran) and Professor Dr. Khalid M. I. Sharbazheri from Sulaimani University (Sulaimani, Kurdistan Region-Iraq) for their help in recognizing and identifying the planktonic species.

References

Agard, P., Omrani, J., Jolivet, L., Whitechurch, H., Vrielynck, B., Spakman, W., Monié, P., Meyer, B., and Wortel, R., 2011. Zagros orogeny: A subduction-dominated process. *Geological Magazine*, 148, pp.692-725.

Alavi, M., 2004. Regional stratigraphy of the Zagros fold-thrust belt of Iran and its proforeland evolution. *American Journal of Science*, 304, pp.1-20.

Al-Banna, N.Y., and Al-Mutwali, M.M., 2008. Microfacies and age determination of the sedimentary sequences within Walash volcano-sedimentary group, Mawat complex, Northeast Iraq. *Tikrit Journal of Pure Science*, 13, pp.46-52.

Al-Mehaidi, H., 1974. *Report on Geological Investigation of Mawat-Chowarta Area*, NE Iraq.

Ali, S.A., and Aswad, K.J., 2013. SHRIMP U-Pb dating of zircon inheritance in Walash arcvolcanic rocks (paleogene age), Zagros suture zone, NE Iraq: New insights into crustal contributions to trachytic andesite generation. *Iraqi National Journal of Earth Sciences*, 13, pp.45-58.

Ali, S.A., 2012. *Geochemistry and Geochronology of Tethyan-arc Related Igneous rocks, NE Iraq, Doctor of Philosophy Thesis, School of Earth and Environmental Sciences*. University of Wollongong. Available from: https://ro.uow.edu.au/theses/3478

Ali, S.A., Buckman, S., Aswad, K.J., Jones, B.G., Ismail, S.A., and Nutman, A.P., 2013. The tectonic evolution of a Neo-Tethyan (eocene-oligocene) island-arc (Walash and Naopurdan groups) in the Kurdistan region of the Northeast Iraqi Zagros suture zone. *Island Arc*, 22, pp.104-125.

Ali, S.A., Sleabi, R.S., Talabani, M.J.A., and Jones, B.G., 2017. Provenance of the Walash-Naopurdan back-arc-arc clastic sequences in the Iraqi Zagros Suture Zone. *Journal of African Earth Sciences*, 125, pp.73-87.

Al-Mehaidi, H., 1974. *Report on Geological Investigation of Mawat-Chowarta area, NE Iraq*.

Al-Qayim, B., Ghafor, I., and Jaff, R., 2012. Contribution to the stratigraphy of the Walash Group, Sulaimani area, Kurdistan, Iraq. *Arabian Journal of Geosciences*, 7, pp.181-192.

Al-Qayim, B., Ghafor, I., and Jaff, R., 2014. Contribution to the stratigraphy of the Walash Group, Sulaimani area, Kurdistan, Iraq. *Arabian Journal of Geosciences*, 7, pp.181-192.

Aragón, E., Pinotti, L., Fernando, D., Castro, A., Rabbia, O., Coniglio, J., Demartis, M., Hernando, I., Cavarozzi, C.E., and Aguilera, Y.E., 2013. The Farallon-Aluk ridge collision with South America: Implications for the geochemical changes of slab window magmas from fore-to back-arc. *Geoscience Frontiers*, 4, pp.377-388.

Asvesta, A., and Dimitriadis, S., 2013. Magma-sediment interaction during the emplacement of syn-sedimentary silicic and mafic intrusions and lavas into and onto Triassic strata (Circum-Rhodope Belt, Northern Greece). *Geologica Carpathica*, 64, pp.181-194.

Aswad, K.J., Aziz, N.R., and Koyi, H.A., 2011. Cr-spinel compositions in serpentinites and their implications for the petrotectonic history of the Zagros Suture Zone, Kurdistan Region, Iraq. *Geological Magazine*, 148(5-6),pp.802-818.

Aswad, K.J.A., Al-Samman, A.H.M., Aziz, N.R.H., and Koyi, A.M.A., 2013. The geochronology and petrogenesis of Walash volcanic rocks, Mawat nappes: Constraints on the evolution of the Northwestern Zagros suture zone, Kurdistan Region, Iraq. *Arabian Journal of Geosciences*, 7, pp.1403-1432.

Austermann, J., and Iaffaldano, G., 2013. The role of the Zagros orogeny in slowing down Arabia-Eurasia convergence since~5 Ma. *Tectonics*, 32, pp.351-363.

Aziz, N.R.H., 1986. *Petrochemistry, Petrogenesis and Tectonic Setting of Spilitic Rocks of Walash Volcanic Sedimentary Group in Qala Diza Area, NE Iraq*. MSc Thesis, Mosul University, Iraq, p.164. (in Arabic).

Aziz, N.R., Aswad, K.J., and Koyi, H.A., 2011. Contrasting settings of serpentinite bodies in the northwestern Zagros Suture Zone, Kurdistan Region, Iraq. *Geological Magazine*, 148(5-6), pp.819-837.

Bann, G.R., Jones, B.G., and Graham, I.T., 2022. A mid-Permian mafic intrusion into wet marine sediments of the lower Shoalhaven Group and its significance in the volcanic history of the Southern Sydney Basin. *Australian Journal of Earth Sciences*, 69, pp.1-17.

Barnes, S.J., and Arndt, N.T., 2019. Distribution and geochemistry of komatiites and basalts through the archean. In: *Earth's Oldest Rocks*. Elsevier, Amsterdam.

Barnes, S.J., and Van Kranendonk, M.J., 2014. Archean andesites in the East Yilgarn craton, Australia: Products of plume-crust interaction? *Lithosphere*, 6, pp.80-92.

Beresford, S., Cas, R., Lahaye, Y., and Jane, M., 2002. Facies architecture of an Archean komatiite-hosted Ni-sulphide ore deposit, Victor, Kambalda, Western Australia: Implications for komatiite lava emplacement. *Journal of Volcanology and Geothermal Research*, 118, pp.57-75.

Berggren, W.A., Pearson, P.N., Huber, B., and Wade, B.S., 2006. *Taxonomy, Biostratigraphy and Phylogeny of Eocene Acarinina*. Cushman Foundation for Foraminiferal Research, New York.

Biske, N., Romashkin, A., and Rychanchik, D., 2004. Proterozoic peperite-structures of Lebestchina. In: *Geology and Mineral Deposits, Proceedings of the Institute of Geology.* Vol. 7. Karelian Research Centre of RAS, Petrozavodsk, pp.193-199.

Blow, W.H., 1979. *The Cainozoic Globigerinida. Atlas*. Brill Archive, Leiden.

Bolton, C., 1958. The Geology of the Ranya Area. Manuscript Report No. 271. GEOSURV, Baghdad.

Boudagher-Fadel, M.K., 2015. *Biostratigraphic and Geological Significance of Planktonic Foraminifera*. Newnes, Oxford.

Boulter, C., 1993. High-level peperitic sills at Rio Tinto, Spain: Implications for stratigraphy and mineralization. *Transactions of the Institution of Mining and Metallurgy. Section B. Applied Earth Scienc*e, 102, pp.30-38.

Branney, M.J., Bonnichsen, B., Andrews, G.D.M., Ellis, B., Barry, T.L., and Mccurry, M., 2008. 'Snake River (SR)-type' volcanism at the yellowstone hotspot track: Distinctive products from unusual, high-temperature silicic super-eruptions. *Bulletin of Volcanology*, 70, pp.293-314.

Bronnimann, P., 1952. Trinidad paleocene and lower eocene globigerinidae. *Bulletins of American Paleontology*, 34, p.134.

Brooks, E.R., 1995. Paleozoic fluidization, folding, and peperite formation, Northern Sierra Nevada, California. *Canadian Journal of Earth Sciences*, 32, pp.314-324.

Brown, D.J., and Bell, B.R., 2007. How do you grade peperites? *Journal of Volcanology and Geothermal Research*, 159, pp.409-420.

Busby-Spera, C.J., and White, J.D., 1987. Variation in peperite textures associated with differing host-sediment properties. *Bulletin of Volcanology*, 49, pp.765-776.

Busby, C.J., Hagan, J.C., Putirka, K., Pluhar, C.J., Gans, P.B., Wagner, D.L., Rood, D., Deoreo, S.B., and Skilling, I., 2008. *The Ancestral Cascades Arc: Cenozoic Evolution of the Central Sierra Nevada (California) and the Birth of the New Plate Boundary*. The Geological Society of America, Boulder.

Cas, R.A.F., Edgar, C., Allen, R.L., Bull, S., Clifford, B.A., Giordano, G., and Wright, J.V., 2001. Influence of magmatism and tectonics on sedimentation in an extensional lake basin: The upper devonian bunga beds, boyd volcanic complex, South-Eastern Australia. *Volcaniclastic Sedimentation in Lacustrine Settings*. Wiley-Blackwell, Hoboken, pp.81-108.

Chen, S., Guo, Z.J., Pe-Piper, G., and Zhu, B.B., 2013. Late paleozoic peperites in West Junggar, China, and how they constrain regional tectonic and palaeoenvironmental settings. *Gondwana Research*, 23, pp.666-681.

Chen, S., Guo, Z., Qi, J., Zhang, Y., Pe-Piper, G., and Piper, D.J.W., 2016. Early permian volcano-sedimentary successions, Beishan, NW China: Peperites demonstrate an evolving rift basin. *Journal of Volcanology and Geothermal Research*, 309, pp.31-44.

Cohen, K.M., Finney, S.C., Gibbard, P.L., and Fan, J., 2021. The ICS international chronostratigraphic chart. *Episodes*, 36, pp.199-204.

Condie, K.C., 1989. Geochemical changes in baslts and andesites across the Archean-Proterozoic boundary: Identification and significance. *Lithos*, 23, pp.1-18.

Condie, K.C., 2005. High field strength element ratios in Archean basalts: A window to evolving sources of mantle plumes? *Lithos*, 79, pp.491-504.

Constenius, K.N., Mcgimsey, R.G., Valencia, V., Ibanex-Mejia, M., and Domanik, K.J., 2017. *Peperite in the Purcell Lava and a Revised Age of the Upper Proterozoic Belt-Purcell Supergroup*. Geological Society of America Abstracts with Programs, Boulder, pp.1-7.

Cushman, J.A., 1925. Some new foraminifera from the Velasco Shale of Mexico. *Contributions from the Cushman Laboratory for Foraminiferal Research*, 1, pp.18-23.

Cushman, J.A., 1942. Eocene, midway, foraminifera from Soldado Rock, Trinidad. *Contributions from the Cushman Laboratory for Foraminiferal Researc*h, 18, pp.1-20.

Dadd, K.A., and Van Wagoner, N.A., 2002. Magma composition and viscosity as controls on peperite texture: An example from Passamaquoddy Bay, Southeastern Canada. *Journal of Volcanology and Geothermal Research*, 114, pp.63-80.

Defant, M.J., and Drummond, M.S., 1990. Derivation of some modern arc magmas by melting of young subducted lithosphere. *Nature*, 347, pp.662-665.

Doyle, M.G., 2000. Clast shape and textural associations in peperite as a guide to hydromagmatic interactions: Upper permian basaltic and basaltic andesite examples from Kiama, Australia. *Australian Journal of Earth Sciences*, 47, pp.167-177.

El Desoky, H.M., and Shahin, T.M., 2020. Characteristics of lava-sediments interactions during emplacement of mid-tertiary volcanism, Northeastern Desert, Egypt: Field geology and geochemistry approach. *Arabian Journal of Geosciences*, 13, p.328.

Elias, Z., Sissakian, V.K., and Al-Ansari, N., 2018. New tectonic activity within Zagros-Taurus belt: A case study from North Iraq using region shuttle radar topography mission (SRTM). *Journal of Earth Sciences and Geotechnical Engineering*, 8, pp.51-63.

Elliott, T., 2003. Tracers of the slab. In: *Geophysical Monograph-American Geophysical Union.* Vol. 138. American Geophysical Union, Washington, D.C., pp.23-46.

Elliott, T., Plank, T., Zindler, A., White, W., and Bourdon, B., 1997. Element transport from slab to volcanic front at the Mariana arc. *Journal of Geophysical Research: Solid Earth*, 102, pp.14991-15019.

English, J.M., Lunn, G.A., Ferreira, L., and Yacu, G., 2015. Geologic evolution of the Iraqi Zagros, and its influence on the distribution of hydrocarbons in the Kurdistan Region. *AAPG Bulletin*, 99, pp.231-272.

Erkül, F., Helvaci, C., and Sözbilir, H., 2006. Olivine basalt and trachyandesite peperites formed at the subsurface/surface interface of a semi-arid lake: An example from the early miocene bigadiç basin, Western Turkey. *Journal of Volcanology and Geothermal Research*, 149, pp.240-262.

Famelli, N., Millett, J.M., Hole, M.J., Lima, E.F., de O.Carmo, I., Jerram, D.A., Jolley, D.W., Pugsley, J.H., and Howell, J.A., 2021. Characterizing the nature and importance of lava-sediment interactions with the aid of field outcrop analogues. *Journal of South American Earth Sciences*, 108, p.103108.

Fontboté, L., 2019. Volcanogenic Zn-Pb±Cu massive sulfide deposits in the upper cretaceous plutono-volcanic arc in central Peru. In: *Proceedings of Proexplo 2019.* Extended Abstracts, Peru.

Goto, Y., and McPhie, J., 1996. A Miocene basanite peperitic dyke at stanley, Northwestern Tasmania, Australia. *Journal of Volcanology and Geothermal Research*, 74, pp.111-120.

Haller, M., and Németh, K., 2009. Cenozoic diatremes in Chubut, Northern Patagonia, Argentina. In: *3ICM International Maar Conference, Malargüe, Argentina, Extended Abstract*.

Hanson, R.E., and Hargrove, U.S., 1999. Processes of magma/wet sediment interaction in a large-scale Jurassic andesitic peperite complex, northern Sierra Nevada, California. *Bulletin of Volcanology*, 60, pp.610-626.

Hanson, R.E., and Wilson, T.J., 1993. Large-scale rhyolite peperites (Jurassic, Southern Chile). *Journal of Volcanology and Geothermal Research*, 54, pp.247-264.

Hanson, R.E., 1991. Quenching and hydroclastic disruption of andesitic to rhyolitic intrusions in a submarine Island-arc sequence, Northern Sierra Nevada, California. *Geological Society of America Bulletin*, 103, pp.804-816.

Hastie, A.R., Kerr, A.C., Pearce, J.A., and Mitchell, S.F., 2007. Classification of altered volcanic Island arc rocks using immobile trace elements: Development of the Th-Co discrimination diagram. *Journal of Petrology*, 48, pp.2341-2357.

Hibbard, M.J., 1995. *Petrography to Petrogenesis*. Macmillan College, London.

Humphris, S.E., and Thompson, G., 1978. Trace element mobility during hydrothermal alteration of oceanic basalts. *Geochimica et Cosmochimica Acta*, 42, pp.127-136.

Iacono Marziano, G., Gaillard, F., and Pichavant, M., 2008. Limestone assimilation by basaltic magmas: An experimental re-assessment and application to Italian volcanoes. *Contributions to Mineralogy and Petrology*, 155, pp.719-738.

Ikeda, Y., 1990. CeN/SrN/SmN: A trace element discriminant for basaltic rocks from different tectonomagmatic environments. *Neues Jahrbuch für Mineralogie Monatshefte*, 4, pp.145-158.

Jassim, S.Z., and Goff, J.C., 2006. *Geology of Iraq*. DOLIN, Sro, Distributed by Geological Society of London, Burlington House.

Karim, K.H., and Hamza, B.J., 2021. Relation between Walash Group and Kolosh Formation: A key to the stratigraphy of the Penjween area. In: *The 1st International Conference for Natural Resources Research Center, Geo Iraq1*, University of Tikrit, Tikrit City.

Koshnaw, R.I., Horton, B.K., Stockli, D.F., Barber, D.E., Tamar-Agha, M.Y., and Kendall, J.J., 2017. Neogene shortening and exhumation of the Zagros fold-thrust belt and foreland basin in the Kurdistan region of northern Iraq. *Tectonophysics*, 694, pp.332-355.

Koyi, A.M.A., 2009. Sr-Nd isotopical significance of Walash volcanic rocks, Mawat area, NE Iraq. *Zanco Journal of Pure and Applied Sciences*, 21, pp.39-45.

Krobicki M., 2018. The earliest Cretaceous (Berriasian) peperites in volcano-sedimentary units of the Ukrainian Carpathians. In: Šujan, M., Csibri, T., Kiss,

P., and Rybár, S. (Eds.): *Environmental, Structural and Stratigraphical Evolution of the Western Carpathians, Abstract Book, 11th ESSEWECA Conference, 29th–30th November 2018*, Bratislava, Slovakia, pp.52–53.

Krobicki, M., Feldman-Olszewska, A., Hnylko, O., and Iwańczuk, J., 2019. Peperites and other volcano-sedimentary deposits (lowermost Cretaceous, Berriasian) of the Ukrainian Carpathians. *Geologica Carpathica*, 70, p.146.

Lieu, W.K., and Stern, R.J., 2019. The robustness of Sr/Y and La/Yb as proxies for crust thickness in modern arcs. *Geosphere*, 15, pp.621-641.

Liu, S., Zhang, J., Li, Q., Zhang, L., Wang, W., and Yang, P., 2012. Geochemistry and U-Pb zircon ages of metamorphic volcanic rocks of the paleoproterozoic lüliang complex and constraints on the evolution of the trans-North China orogen, North China craton. *Precambrian Research*, 222, pp.173-190.

Loeblich, A.R., and Tappan, H.N., 1957. Planktonic foraminifera of paleocene and early eocene age from the. *Bulletin United States National Museum*, 215, pp.173-198.

Martin, L.T., 1943. *Eocene Foraminifera from the Type Lodo Formation, Fresno County, California*, Stanford University Press, Redwood City.

Martin, U., and Németh, K., 2007. Blocky versus fluidal peperite textures developed in volcanic conduits, vents and crater lakes of phreatomagmatic volcanoes in mio/pliocene volcanic fields of Western Hungary. *Journal of Volcanology and Geothermal Research*, 159, pp.164-178.

Mawson, J.F., White, J., and Palin, J.M., 2020. Contemporaneously emplaced submarine volcaniclastic deposits and pillow lavas from multiple sources in the Island arc brook street Terrane, Southland, New Zealand. *New Zealand Journal of Geology and Geophysics*, 63, pp.562-577.

McLennan, S.M., 1989. Rare earth elements in sedimentary rocks: Influence of provenance and sedimentary process. *Reviews in Mineralogy*, 21, pp.169-200.

Mcphie, J., 1993. The tennant creek porphyry revisited: A synsedimentary sill with peperite margins, early proterozoic, Northern Territory. *Australian Journal of Earth Sciences*, 40, pp.545-558.

Memtimin, M., Zhang, Y., Furnes, H., Pe-Piper, G., Piper, D.J.W., and Guo, Z., 2020. Facies architecture of a subaqueous volcano-sedimentary succession on Bogda Mountains, NW China-evidence of extension in late carboniferous. *Geological Journal*, 55, pp.3097-3111.

Mercurio, E.C., 2011. *Processes, Products and Depositional Environments of Ice-Confined Basaltic Fissure Eruptions: A Case Study of the Sveifluhals Volcanic Complex, SW Iceland.* University of Pittsburgh, Pittsburgh.

Miyashiro, A., 1974. Volcanic rock series in island arcs and active continental margins. *American Journal of Science*, 274, pp.321-355.

Mohammad, Y.O., Cornell, D.H., Qaradaghi, J.H., and Mohammad, F.O., 2014. Geochemistry and Ar-Ar muscovite ages of the Daraban Leucogranite, Mawat Ophiolite, Northeastern Iraq: Implications for Arabia-Eurasia continental collision. *Journal of Asian Earth Sciences*, 86, pp.151-165.

Morozova, V.G., 1939. K stratigrafii verkhnego mela i paleogena Embenskoi oblasti po faune foraminifer [On the stratigraphy of the upper cretaceous and paleogene of Emba region according to the foraminiferal fauna]. *Biulleten Moskovskogo Obshchestva Ispytatelei Prirody, Otdel Geologicheskii*, 17, pp.59-86.

Moulton, B.J.A., Fowler, A.D., Ayer, J.A., Berger, B.R., and Mercier-Langevin, P., 2011. Archean subqueous high-silica rhyolite coulées: Examples from the Kidd-Munro assemblage in the abitibi subprovince. *Precambrian Research*, 189, pp.389-403.

Mueller, W.U., Garde, A.A., and Stendal, H., 2000. Shallow-water, eruption-fed, mafic pyroclastic deposits along a paleoproterozoic coastline: Kangerluluk volcano-sedimentary sequence, southeast Greenland. *Precambrian Research*, 101, pp.163-192.

Nayudu, Y.R., 1971. Geologic implications of microfossils in submarine volcanics. *Bulletin Volcanologique*, 35, pp.402-423.

Nemeth, K., Breitkreutz, C., and Wilke, H.G., 2004. *Volcano-sedimentary Successions within an Intra-arc Related Jurassic Large Igneous Province (LIP): La Negra Formation, Northern Chile (a Preliminary Scientific Report on the Br 997/22-1 DFG Pilot Project)*.

Nesbitt, H.W., and Young, G.M., 1982. Early proterozoic climates and plate motions inferred from major element chemistry of lutites. *Nature*, 299, pp. 715-717.

Nouri, F., Asahara, Y., Azizi, H., Yamamoto, K., and Tsuboi, M., 2017. Geochemistry and petrogenesis of the eocene back arc mafic rocks in the Zagros suture zone, Northern Noorabad, Western Iran. *Geochemistry*, 77, pp.517-533.

Olsson, R.K., Berggren, W.A., Hemleben, C., and Huber, B.T., 1999. *Atlas of Paleocene Planktonic Foraminifera*. Smithsonian Institution Press, Washington, D.C.

Palinkaš, L.A., Bermanec, V., Šoštarić, S.B., Kolar-Jurkovšek, T., Palinkaš, S.S., Molnar, F., and Kniewald, G., 2008. Volcanic facies analysis of a subaqueous basalt lava-flow complex at Hruškovec, NW Croatia-Evidence of advanced rifting in the Tethyan domain. *Journal of Volcanology and Geothermal Research*, 178, pp.644-656.

Parr, W.J., 1938. Upper eocene foraminifera from deep borings in King's park, Perth, Western Australia. *Journal of the Royal Society of Western Australia*, 24, pp.69-101.

Pearce, J.A., 1982. In: Thorpe, R.S., editor. *En: Andesites: Orogenic Andesites and Related Rocks*. John Wiley and Sons, Hoboken.

Pearce, J.A., and Cann, J.R., 1973. Tectonic setting of basic volcanic rocks determined using trace element analyses. *Earth and Planetary Science Letters*, 19, pp.290-300.

Pearce, J.A., 1983. *Role of the Sub-Continental Lithosphere in Magma Genesis at Active Continental Margins*. Shiva Cheshire, UK, Cheshire.

Pearce, J.A., 1996. A user's guide to basalt discrimination diagrams. In: *Trace element Geochemistry of Volcanic Rocks: Applications for Massive Sulphide Exploration.* Vol. 12. Geological Association of Canada, Short Course Notes, Canada, p.113.

Pearce, J.A., van der Laan, S.R., Arculus, R.J., Murton, B.J., Ishii, T., Peate, D.W., and Parkinson, I.J., 1992. Boninite and harzburgite from Leg 125 (Bonin-Mariana forearc): A case study of magma genesis during the initial stages of subduction. In: *Proceedings of the Ocean Drilling Program, Scientific Results*. Ocean Drilling Program, College Station, TX, pp.623-659.

Pearce, T.H., Gorman, B.E., and Birkett, T.C., 1977. The relationship between major element chemistry and tectonic environment of basic and intermediate volcanic rocks. *Earth and Planetary Science Letters*, 36, pp.121-132.

Perfit, M.R., Gust, D.A., Bence, A.E., Arculus, R.J., and Taylor, S.R., 1980. Chemical characteristics of island-arc basalts: Implications for mantle sources. *Chemical Geology*, 30, pp.227-256.

Philpotts, A.R., and Ague, J.J., 2022. *Principles of Igneous and Metamorphic Petrology*. Cambridge University Press, Cambridge.

Rawlings, D.J., 1993. Mafic peperite from the gold creek Volcanics in the middle proterozoic McArthur Basin, Northern Territory. *Australian Journal of Earth Sciences*, 40, pp.109-113.

Rogers, G., and Hawkesworth, C.J., 1989. A geochemical traverse across the North Chilean Andes: Evidence for crust generation from the mantle wedge. *Earth and Planetary Science Letters*, 91, pp.271-285.

Ross, P.S., and Bédard, J.H., 2009. Magmatic affinity of modern and ancient subalkaline volcanic rocks determined from trace-element discriminant diagrams. *Canadian Journal of Earth Sciences*, 46, pp.823-839.

Ryerson, F.J., and Watson, E.B., 1987. Rutile saturation in magmas: Implications for Ti-Nb-Ta depletion in island-arc basalts. *Earth and Planetary Science Letters*, 86, pp.225-239.

Saunders, A.D., and Tarney, J., 1979. The geochemistry of basalts from a back-

arc spreading centre in the East Scotia Sea. *Geochimica et Cosmochimica Acta*, 43, pp.555-572.

Scrope, G.P., 1827. *Memoir on the Geology of Central France: Including the Volcanic Formations of Auvergne, the Velay, and the Vivarsais*. Longman, Rees, Orme, Brown, and Green, London.

Shuto, K., Nohara-Imanaka, R., Sato, M., Takahashi, T., Takazawa, E., Kawabata, H., Takanashi, K., Ban, M., Watanabe, N., and Fujibayashi, N., 2015. Across-arc variations in geochemistry of oligocene to quaternary basalts from the NE Japan arc: Constraints on source composition, mantle melting and slab input composition. *Journal of Petrology*, 56, pp.2257-2297.

Sinha, K.K., Pandey, P., Bhairam, C.L., and Parihar, P.S., 2011. Peperite occurrence and its implications on origin and temporal development of the proterozoic Dhala Basin, Mohar area, Shivpuri district, Madhya Pradesh. *Journal of the Geological Society of India*, 77, pp.183-189.

Skilling, I.P., White, J.D.L., and Mcphie, J., 2002. Peperite: A review of magma-sediment mingling. *Journal of Volcanology and Geothermal Research*, 114, pp.1-17.

Slovenec, D., Lugovic, B., and Vlahovic, I., 2010. Geochemistry, petrology and tectonomagmatic significance of basaltic rocks from the ophiolite mélange at the NW external-internal dinarides junction (Croatia). *Geologica Carpathica*, 61, pp.273-292.

Sohn, C., and Sohn, Y.K., 2019. Distinguishing between primary and secondary volcaniclastic deposits. *Scientific Reports*, 9, p.12425.

Squire, R.J., and Mcphie, J., 2002. Characteristics and origin of peperite involving coarse-grained host sediment. *Journal of Volcanology and Geothermal Research*, 114, pp.45-61.

Stern, R.J., 2010. *The Anatomy and Ontogeny of Modern Intra-Oceanic Arc Systems.* Vol. 338. Geological Society, London, Special Publications, London, pp.7-34.

Sun, S.S., and McDonough, W.F., 1989. *Chemical and Isotopic Systematics of Oceanic Basalts: Implications for Mantle Composition and Processes*. Vol. 42. Geological Society, London, Special Publications, London, pp.313-345.

Templeton, J.H., and Hanson, R.E., 2003. Jurassic submarine arc-apron deposits and associated Magma/Wet-sediment interaction, northern Sierra Nevada, California. *Journal of Volcanology and Geothermal Research*, 128, pp.299-326.

Thompson, G., 1991. Metamorphic and hydrothermal processes: Basalt-seawater interactions. In: *Oceanic Basalts.* Springer, Berlin.

Toulmin, L.D., 1941. Eocene smaller foraminifera from the Salt Mountain Limestone of Alabama. *Journal of Paleontology*, 15, pp.567-611.

Wade, B.S., Pearson, P.N., Berggren, W.A., and Pälike, H., 2011. Review and revision of cenozoic tropical planktonic foraminiferal biostratigraphy and calibration to the geomagnetic polarity and astronomical time scale. *Earth-Science Reviews*, 104, pp.111-142.

Waichel, B.L., de Lima, E.F., Sommer, C.A., and Lubachesky, R., 2007. Peperite formed by lava flows over sediments: An example from the central paraná continental flood basalts, Brazil. *Journal of Volcanology and Geothermal Research*, 159, pp.343-354.

Walker, G.P.L., 1992. Morphometric study of pillow-size spectrum among pillow lavas. *Bulletin of Volcanology*, 54, pp.459-474.

Wang, T., Wang, Z., Yan, Z., Ma, Z., He, S., Fu, C., and Wang, D., 2016. Geochronological and geochemical evidence of amphibolite from the Hualong Group, Northwest China: Implication for the early Paleozoic accretionary tectonics of the Central Qilian belt. *Lithos*, 248, pp.12-21.

White, J., and Houghton, B., 2006. Primary volcaniclastic rocks. *Geology*, 34, pp.677-680.

White, J.D.L., and Busby-Spera, C.J., 1987. Deep marine arc apron deposits and syndepositional magmatism in the Alisitos Group at Punta Cono, Baja California, Mexico. *Sedimentology*, 34, pp.911-927.

White, J.D.L., Mcphie, J., and Skilling, I., 2000. Peperite: A useful genetic term. *Bulletin of Volcanology*, 62, pp.65-66.

White, M.P., 1928. Some index foraminifera of the Tampico Embayment area of Mexico. Part I. *Journal of Paleontology*, 2, pp.177-215.

Whitney, D.L., and Evans, B.W., 2010. Abbreviations for names of rock-forming minerals. *American Mineralogist*, 95, pp.185-187.

Wilson, A.H., and Grant, C.E., 2006. *Physical Volcanology and Compositions of the Basaltic Lavas in the Archean Nzuse Group, White Mfolozi Inlier, South Africa*. Geological Society of America, Boulder.

Wilson, T.J., and Hanson, R.E., 1991. Submarine rhyolitic volcanism in a Jurassic proto-marginal basin; southern Andes, Chile and Argentina. In: *Andean Magmatism and its Tectonic Setting*. Vol. 265. Geological Society of America, Boulder, p.13.

Winchester, J.A., and Floyd, P.A., 1977. Geochemical discrimination of different magma series and their differentiation products using immobile elements. *Chemical Geology*, 20, pp.325-343.

Wood, D.A., Joron, J.L., Treuil, M., Norry, M., and Tarney, J., 1979. Elemental and Sr isotope variations in basic lavas from Iceland and the surrounding ocean floor. *Contribibution to Mineralogy and Petrology*, 70, pp.319-339.

Zhu, B., Guo, Z., Zhang, Z., and Cheng, F., 2014. Peperites in the permian tarim large igneous province in Northwest China and their constraints on the local eruption environments. *Science China Earth Sciences*, 57, pp.2914-2921.